

Variational and parquet-diagram calculations for neutron matter.

I. Structure and Energetics.

E. Krotscheck and J. Wang

*Department of Physics, University at Buffalo, SUNY Buffalo NY 14260 and
Institut für Theoretische Physik, Johannes Kepler Universität, A 4040 Linz, Austria*

Abstract

We develop the variational/parquet diagram approach to the structure of nuclear systems with strongly state-dependent interactions. For that purpose, we combine ideas of the general Jastrow-Feenberg variational method and the local parquet-diagram theory for bosons with state-dependent interactions (R. A. Smith and A. D. Jackson, Nucl. Phys. **476**, 448 (1988)). The most tedious aspect of variational approaches, namely the symmetrization of an operator dependent variational wave function, is thereby avoided. We carry out calculations for neutron matter interacting via the Reid and Argonne v_6 models of the nucleon-nucleon interaction. While the equation of state is a rather robust quantity that comes out reasonably well even in very simplistic approaches, we show that effective interactions, which are the essential input for calculating dynamic properties, depend sensitively on the quality of the treatment of the many-body problem.

I. INTRODUCTION

Realistic nucleon-nucleon interactions depend on the relative spin, isospin, orientations, and angular momenta of the nucleons involved. Popular phenomenological models [1–5] represent the interaction in the form of a sum of local functions, times correlation operators, *i.e.*

$$\hat{v}(i, j) = \sum_{\alpha=1}^n v_{\alpha}(r_{ij}) \hat{O}_{\alpha}(i, j), \quad (1.1)$$

where $r_{ij} = |\mathbf{r}_i - \mathbf{r}_j|$ is the distance between particles i and j , and the $O_{\alpha}(i, j)$ are operators acting on the spin, isospin, and possibly angular momentum variables of the individual particles. According to the number of operators n , the potential model is referred to as a v_n model potential. Semi-realistic models for nuclear matter keep at least 6 operators, but up to 28 operators have been included [5] in the sum (1.1).

The six base operators are

$$\begin{aligned} O_1(i, j; \hat{\mathbf{r}}_{ij}) &\equiv O_c = \mathbb{1}, \\ O_3(i, j; \hat{\mathbf{r}}_{ij}) &\equiv (\boldsymbol{\sigma}_i \cdot \boldsymbol{\sigma}_j), \\ O_5(i, j; \hat{\mathbf{r}}_{ij}) &\equiv S(i, j; \hat{\mathbf{r}}_{ij}) \equiv 3(\boldsymbol{\sigma}_i \cdot \hat{\mathbf{r}}_{ij})(\boldsymbol{\sigma}_j \cdot \hat{\mathbf{r}}_{ij}) - \boldsymbol{\sigma}_i \cdot \boldsymbol{\sigma}_j, \\ O_{2n}(i, j; \hat{\mathbf{r}}_{ij}) &= O_{2n-1}(i, j; \hat{\mathbf{r}}_{ij}) \boldsymbol{\tau}_1 \cdot \boldsymbol{\tau}_2. \end{aligned} \quad (1.2)$$

where $\hat{\mathbf{r}}_{ij} = \mathbf{r}_{ij}/r_{ij}$. These operators are referred to as central, spin, tensor, isospin, spin-isospin and tensor-isospin operators, respectively. The arguments i, j and $\hat{\mathbf{r}}_{ij}$ of state-dependent functions will be omitted for simplicity when no ambiguity arises.

For simple, state-independent interactions as appropriate for electrons or quantum fluids, the Jastrow-Feenberg ansatz [6] for the wave function

$$\Psi_0 = \prod_{\substack{i, j=1 \\ i < j}}^N f(r_{ij}) \Phi_0 \quad (1.3)$$

and its logical generalization to multiparticle correlation functions has been extremely successful. Here Φ_0 is a model state describing the statistics and, when appropriate, the geometry of the system; for fermions it is normally taken as a Slater determinant. One of the reasons for the success of this wave function is that it provides a reasonable upper bound for the ground state energy

$$E_0 = \frac{\langle \Psi_0 | H | \Psi_0 \rangle}{\langle \Psi_0 | \Psi_0 \rangle}. \quad (1.4)$$

It has therefore been applied in both semi-analytic calculations [6] as well as early Monte Carlo calculations [7, 8] and is still being used as an importance sampling function for diffusion and Green’s Functions Monte Carlo computations [9, 10]. Semi-analytic methods employ diagram expansions and integral equation methods – specifically the hypernetted chain (HNC) summations [11, 12] or its fermion versions (FHNC) [13, 14] – for the calculation of physically interesting quantities.

In particular, this approach permits an unconstrained optimization of the assumed correlation functions,

$$\frac{\delta E_0}{\delta f_n}(\mathbf{r}_1, \dots, \mathbf{r}_n) = 0, \quad (1.5)$$

in which case the method is referred to as the (Fermi-)Hypernetted-Chain-Euler-Lagrange (F)HNC-EL procedure. It has been a particularly important insight that the HNC-EL method corresponds, for bosons, to a self-consistent summation of all ring and ladder diagrams of perturbation theory – the so-called “parquet” diagrams [15–17]. To carry out these summations, specific local approximations are made, but the upper-bound property for the energy makes sure that one has achieved the best approximation for the computational price one is willing to pay.

The Jastrow-Feenberg ansatz (1.3) is insufficient for dealing with realistic nucleon-nucleon interactions of the form (1.1). A logical generalization of the Jastrow-Feenberg wave function (1.3) is the symmetrized operator product [18, 19]

$$\Psi_0^{\text{SOP}} = \mathcal{S} \left[\prod_{\substack{i,j=1 \\ i < j}}^N \hat{f}(i, j) \right] \Phi_0, \quad (1.6)$$

where

$$\hat{f}(i, j) = \sum_{\alpha=1}^n f_{\alpha}(r_{ij}) O_{\alpha}(i, j) \quad (1.7)$$

and \mathcal{S} stands for symmetrization. Unfortunately, the need to symmetrize the correlations figuratively opens Pandora’s box. Not surprisingly, only limited success has been achieved [18–20]. In fact, it is not even clear how to choose the correlation functions $f_{\alpha}(r_{ij})$ because, due to the symmetrization, components $v_{\alpha}(r)$ of the interaction are multiplied, in the energy expectation value (1.4), by products of correlation functions $f_{\beta}(r)f_{\gamma}(r)$ with $\beta \neq \alpha$ and $\gamma \neq \alpha$ [21]. This makes the use of simplistic choices of the correlation functions like the “low-order constrained variational (LOCV) method” [22, 23] highly problematic if the interactions in the different operator channels are very different [21] and sufficiently high-order commutators

are included. Hence, only very simple implementations – the so-called “single operator chain (SOC)” approximation [24] – have been carried out. Moreover, the complicated structure of commutator terms makes the identification with Feynman diagrams nontransparent.

In view of this situation, Smith and Jackson [25] started from the idea of localized parquet-diagram summations and implemented the procedure for a fictive system of bosonic nucleons interacting via a v_6 interaction. It turned out that the equations derived were identical to those one would obtain in a bosonic version of the summation method of Fantoni and Rosati [18], which simply ignored the fact that the individual pair correlation operators $\hat{f}(i, j)$ do not commute. In other words, the problem of the importance of commutator diagrams does not go away, but the idea of parquet-diagram summations promises a clearer procedure to deal with these effects without having to go through the development of a full variational procedure.

Therefore we adopt here the ideas of Smith and Jackson and generalize them to Fermi systems. To that end, in the next section we will first review how the connections between the HNC-EL equations of the Jastrow-Feenberg theory and parquet-diagram summations are established. We will then show how specific equations from the FHNC-EL theory for state-independent correlations can be derived from corresponding sets of parquet diagrams. Specifically, we will focus on ring diagrams and the Bethe-Goldstone equation. Once the connections have been established, we can go on and formulate the method for fermions with a v_6 interaction.

We will restrict ourselves to neutron matter in our applications for two reasons: First, we feel that the problem of commutator diagrams which would, in the language of parquet theory, correspond to “twisted” ladder rungs, is solved. Additionally, it has been pointed out [26] that the spin-orbit force, which is omitted in the v_6 models, plays an important role in nuclear matter calculations near isospin symmetry. We will demonstrate the importance of both the state-dependence of the correlations and the non-locality introduced by the Pauli principle. On the other hand, we do not attempt an exhaustive comparison with previous neutron-matter calculations as carried out in Ref. 26. Rather, we concentrate on the technical implementations of parquet theory and its connections to FHNC.

II. VARIATIONAL AND PARQUET THEORY

A. Bosons in a nutshell

In this subsection we review very briefly the optimized variational method (“HNC-EL”) for bosons and the “local parquet summations,” because these equations have a very familiar structure and can be derived with minimal approximations from various basic theories. Skipping the technical details that can be found in original papers and pedagogical expositions, we display the resulting equations.

The static structure function $S(q)$ is expressed in terms of a Bogoliubov equation

$$S(q) = \frac{1}{\sqrt{1 + \frac{2\tilde{V}_{\text{p-h}}(q)}{t(q)}}} \quad (2.1)$$

in terms of a self-consistently determined “particle-hole” interaction $V_{\text{p-h}}$. Having defined a dimensionless Fourier transform by including a density factor ρ , i.e.,

$$\tilde{f}(q) = \rho \int d^3r e^{i\mathbf{q}\cdot\mathbf{r}} f(r), \quad (2.2)$$

this effective interaction takes the specific form

$$V_{\text{p-h}}(r) = g(r) [v(r) + \Delta V_e(r)] + \frac{\hbar^2}{m} \left| \nabla \sqrt{g(r)} \right|^2 + [g(r) - 1] w_{\text{I}}(r), \quad (2.3)$$

$$\tilde{w}_{\text{I}}(q) = -t(q) \left[1 - \frac{1}{S(q)} \right]^2 \left[S(q) + \frac{1}{2} \right]. \quad (2.4)$$

In the language of Jastrow-Feenberg theory, the term $\Delta V_e(r)$ accounts for the contribution from “elementary diagrams” and multiparticle correlations [30], whereas in terms of parquet-diagram theory it is the contribution of diagrams that are both particle-particle and particle-hole irreducible [31].

A few algebraic manipulations show that the pair distribution function satisfies the coordinate-space equation [32]

$$\frac{\hbar^2}{m} \nabla^2 \sqrt{g(r)} = [v(r) + \Delta V_e(r) + w_{\text{I}}(r)] \sqrt{g(r)}. \quad (2.5)$$

Eq. (2.5) is recognized as the boson Bethe-Goldstone equation in terms of the interaction $v(r) + \Delta V_e(r) + w_{\text{I}}(r)$. This observation led Sim, Woo, and Buchler [33] to the conclusion that

“it appears that the optimized Jastrow function is capable of summing all rings and ladders, and partially all other diagrams, to infinite order.” In fact, the form of the equations can be obtained by *demanding* that the pair distribution function $g(r)$ satisfies both the Bogoliubov equation (2.1) and the Bethe-Goldstone equation (2.5) [28]; the only quantity undetermined by that requirement is $\Delta V_e(r)$.

Since we will heavily rely on the derivations and localization procedures of parquet-diagram theory, let us briefly review the relevant steps. First, the Bogoliubov equation (2.1) is derived from a random-phase approximation (RPA) equation for the density-density response function

$$\chi(q, \omega) = \frac{\chi_0(q, \omega)}{1 - \tilde{V}_{p-h}(q)\chi_0(q, \omega)} \quad (2.6)$$

$$S(q) = - \int_0^\infty \frac{d\hbar\omega}{\pi} \mathcal{I}m \chi(q, \omega), \quad (2.7)$$

in terms of a *local* and *energy-independent* particle-hole interaction $\tilde{V}_{p-h}(q)$. Here

$$\chi_0(q, \omega) = \frac{2t(q)}{(\hbar\omega + i\eta)^2 - t^2(q)}, \quad (2.8)$$

with $t(q) = \frac{\hbar^2 q^2}{2m}$, is the particle-hole propagator of non-interacting bosons. Eq. (2.7) defines an *energy dependent* effective interaction

$$\tilde{W}(q, \omega) = \frac{\tilde{V}_{p-h}(q)}{1 - \tilde{V}_{p-h}(q)\chi_0(q, \omega)}. \quad (2.9)$$

An *energy independent* effective interaction $\tilde{W}(q)$ is then defined such that it leads to the same $S(q)$, *i.e.*

$$\begin{aligned} S(q) &= - \int_0^\infty \frac{d\hbar\omega}{\pi} \mathcal{I}m \frac{\chi_0(q, \omega)}{1 - \tilde{V}_{p-h}(q)\chi_0(q, \omega)} \\ &= - \int_0^\infty \frac{d\hbar\omega}{\pi} \mathcal{I}m \left[\chi_0(q, \omega) + \chi_0^2(q, \omega)\tilde{W}(q, \omega) \right] \\ &\stackrel{!}{=} - \int_0^\infty \frac{d\hbar\omega}{\pi} \mathcal{I}m \left[\chi_0(q, \omega) + \chi_0^2(q, \omega)\tilde{W}(q) \right], \end{aligned} \quad (2.10)$$

where the last line defines $\tilde{W}(q)$. Carrying out the integration leads to

$$\tilde{W}(q) = -t(q)(S(q) - 1). \quad (2.11)$$

The particle-hole reducible part

$$\tilde{w}_I(q) = \tilde{W}(q) - \tilde{V}_{p-h}(q) \quad (2.12)$$

of $\widetilde{W}(q)$ so defined is then exactly the induced interaction (2.4). This local $w_I(r)$ then supplements the bare interaction in the Bethe-Goldstone equation.

It is relatively straightforward to generalize the procedure to interactions with spin and tensor components that are needed for nuclear systems [25].

B. Fermions with state-independent interactions

We discuss here the simplest implementation of the FHNC theory that is compatible with the variational problem, called the FHNC//0 approximation. This version has quantitative deficiencies, in particular at high densities, but it permits the clearest connection to the summation of ring and ladder diagrams of parquet theory. The implementation and relevance of higher order exchange corrections will be discussed below in Section III D.

In the FHNC//0 approximation, the generalization of Eq. (2.1) is

$$S(q) = \frac{S_F(q)}{\sqrt{1 + 2\frac{S_F^2(q)}{t(q)}\tilde{V}_{p-h}(q)}}. \quad (2.13)$$

where

$$S_F(q) = \begin{cases} \frac{3q}{4k_F} - \frac{q^3}{16k_F^3}, & q < 2k_F; \\ 1, & q \geq 2k_F. \end{cases} \quad (2.14)$$

is the static structure function of the non-interacting Fermi gas.

In this approximation, the effective interaction $\tilde{V}_{p-h}(q)$ is approximated by the “direct” part of the particle-hole interaction, $\tilde{V}_{p-h}(q) \approx \tilde{V}_{dd}(q)$ in the language of the FHNC summations [34, 35]. This quantity is structurally identical to that for bosons, *i.e.*,

$$V_{p-h}(r) = V_{CW}(r) + \Gamma_{dd}(r)w_I(r). \quad (2.15)$$

Here

$$V_{CW}(r) = (1 + \Gamma_{dd}(r))v(r) + \frac{\hbar^2}{m} \left| \nabla \sqrt{1 + \Gamma_{dd}(r)} \right|^2 \quad (2.16)$$

is the “Clark-Westhaus” effective interaction [34], $\Gamma_{dd}(r)$ is the so-called direct correlation function, and $w_I(r)$ is the “induced interaction”

$$\begin{aligned} \tilde{w}_I(q) &= -V_{p-h}(q) - t_F(q)\tilde{\Gamma}_{dd}(q) \\ &= -t(q) \left[\frac{1}{S_F(q)} - \frac{1}{S(q)} \right]^2 \left[\frac{S(q)}{S_F(q)} + \frac{1}{2} \right], \end{aligned} \quad (2.17)$$

where we have abbreviated

$$t_F(q) = \frac{t(q)}{S_F(q)} \quad (2.18)$$

for future reference. In FHNC//0 approximation, the static structure function $S(q)$ and the direct correlation function $\tilde{\Gamma}_{\text{dd}}(q)$ are related by

$$S(q) = S_F(q) \left[1 + \tilde{\Gamma}_{\text{dd}}(q) S_F(q) \right]. \quad (2.19)$$

The Bose limit is obtained by setting $S_F(q) \rightarrow 1$. Note that the Fourier transform of Eq. (2.19) does not give a useful expression for the pair distribution function. This feature, its cause, and how to overcome it has been discussed in many places; see, for example, Refs. 35 and 29.

To derive the equation determining the short-ranged structure of the correlations, we begin with Eq. (2.17) which, using Eqs. (2.15) and (2.16), can be written as

$$\begin{aligned} V_{\text{p-h}}(r) + w_{\text{I}}(r) &= (1 + \Gamma_{\text{dd}}(r)) [v(r) + w_{\text{I}}(r)] \\ &\quad + \frac{\hbar^2}{m} \left| \nabla \sqrt{1 + \Gamma_{\text{dd}}(r)} \right|^2 \\ &= - \left[t_F(q) \tilde{\Gamma}_{\text{dd}}(q) \right]^{\mathcal{F}}(r) \end{aligned} \quad (2.20)$$

(*cf.* Eq. (2.62)) of Ref. 36). This expression can in turn be rewritten in coordinate space as

$$\begin{aligned} &\sqrt{1 + \Gamma_{\text{dd}}(r)} \left[-\frac{\hbar^2}{2m} \nabla^2 + v(r) + w_{\text{I}}(r) \right] \sqrt{1 + \Gamma_{\text{dd}}(r)} \\ &= \left[t_F(q) (S_F(q) - 1) \tilde{\Gamma}_{\text{dd}}(q) \right]^{\mathcal{F}}(r), \end{aligned} \quad (2.21)$$

where $[\dots]^{\mathcal{F}}$ stands for the Fourier transform (2.2).

The right-hand side of Eq. (2.21) is evidently zero for bosons, and the Euler equation is a simple zero-energy Schrödinger equation where the bare interaction is supplemented by the induced potential. For fermions, the right-hand side alters [37] the short-ranged behavior of the correlation function $\Gamma_{\text{dd}}(r)$, and hence the short-ranged behavior of the pair distribution function $g(r)$.

C. Connections between FHNC and parquet diagrams

1. Rings

The expression (2.13) reduces to the Bogoliubov equation for the case of bosons, with $S_F(q) = 1$. For fermions, we must identify $\chi_0(q, \omega)$ with the Lindhard function

$$\chi_0(q, \omega) = \frac{2}{N} \sum_{\mathbf{h}} \frac{n(h)\bar{n}(|\mathbf{h} + \mathbf{q}|)(t(|\mathbf{h} + \mathbf{q}|) - t(h))}{(\hbar\omega + i\eta)^2 - (t(|\mathbf{h} + \mathbf{q}|) - t(h))^2}, \quad (2.22)$$

where $n(q) = \theta(k_F - q)$ is the Fermi distribution and $\bar{n}(q) = 1 - n(q)$. Consistent with the convention (2.2) (for which $\tilde{V}_{p-h}(q)$ has the dimension of an energy), we have defined the density-density response function slightly differently than usual [38], namely such that it has the dimension of an inverse energy.

The energy integration can no longer be carried out analytically. Nevertheless, we anticipate that Eq. (2.13) can also be derived for fermions from the random-phase approximation (2.7) for the dynamic structure function. Given any function $f(\mathbf{p}, \mathbf{h})$ depending on a “hole momentum” $|\mathbf{h}| < k_F$ and a “particle momentum” $\mathbf{p} = \mathbf{h} + \mathbf{q}$ with $|\mathbf{p}| > k_F$, we may define its Fermi-sea average by

$$\begin{aligned} \langle f(\mathbf{p}, \mathbf{h}) \rangle (q) &= \frac{\sum_{\mathbf{h}} \bar{n}(|\mathbf{h} + \mathbf{q}|)n(h)f(\mathbf{h} + \mathbf{q}, \mathbf{h})}{\sum_{\mathbf{h}} \bar{n}(|\mathbf{h} + \mathbf{q}|)n(h)} \\ &= \frac{1}{S_F(q)} \int \frac{d^3h}{V_F} \bar{n}(|\mathbf{h} + \mathbf{q}|)n(h)f(\mathbf{h} + \mathbf{q}, \mathbf{h}), \end{aligned} \quad (2.23)$$

where V_F is the volume of the Fermi sphere. In particular, we find

$$\langle t(|\mathbf{h} + \mathbf{q}|) - t(h) \rangle (q) = \frac{t(q)}{S_F(q)} = t_F(q) \quad (2.24)$$

which justifies our identification of $t_F(q)$ as an “average” kinetic energy of the non-interacting Fermi system.

Eq. (2.13) can then be obtained by approximating the particle-hole energies $t(|\mathbf{h} + \mathbf{q}|) - t(h)$ in the Lindhard function (2.22) by the “average” kinetic energy $t_F(q)$, leading to a “collective” Lindhard function,

$$\chi_0^{\text{coll}}(q, \omega) = \frac{2t(q)}{(\hbar\omega + i\eta)^2 - t_F^2(q)}. \quad (2.25)$$

This approximation is occasionally also referred to as a “one-pole approximation” or “mean spherical approximation”. Alternative rationalizations of the collective approximation for the Lindhard function may be found in Ref. 29. The frequency integration (2.7) can then be carried out analytically and leads to equation (2.13).

2. Ladder Rungs

The analysis leading to the identification of a local, energy-independent induced interaction $\tilde{w}_I(q)$ based on an energy-dependent interaction of the form (2.9) is exactly the same for fermions and for bosons. Following Refs. 15, 16, we define a *local* effective interaction through the condition (2.10),

$$S(q) = S_F(q) - \tilde{W}(q) \int_0^\infty \frac{d\hbar\omega}{\pi} \mathcal{I}m\chi_0^2(q, \omega). \quad (2.26)$$

For further reference, let

$$\int_0^\infty \frac{d\hbar\omega}{\pi} \mathcal{I}m\chi_0^2(q, \omega) \equiv \frac{S_F^3(q)}{t(q)\lambda(q)}; \quad (2.27)$$

we then have

$$\tilde{W}(q) = -t_F(q)\lambda(q) \frac{S(q) - S_F(q)}{S_F^2(q)}. \quad (2.28)$$

The frequency integral in Eq. (2.27) can be carried out analytically [38]. In the “collective approximation” (2.25) for $\chi_0(q, \omega)$, we obtain $\lambda(q) = 1$ and we recover the induced interaction $\tilde{w}_I(q)$ from Eq. (2.17).

An issue that needs to be addressed when moving from the Jastrow-Feenberg description to parquet diagrams concerns the definition of $\tilde{\Gamma}_{dd}(q)$. In FHNC//0 we can obtain this quantity from $S(q)$ via Eq. (2.19). To construct the equivalent of this relationship in parquet theory, we go back to Eq. (2.26). There we should identify

$$\tilde{\Gamma}_{dd}(q)S_F^2(q) = -\tilde{W}(q) \int_0^\infty \frac{d\hbar\omega}{\pi} \mathcal{I}m\chi_0^2(q, \omega) = S(q) - S_F(q). \quad (2.29)$$

Accordingly, the relationship between $\tilde{\Gamma}_{dd}(q)$ and $S(q)$ is always given by Eq. (2.19).

3. Ladders

The final objective is to identify the coordinate-space equation with a local approximation of the Bethe-Goldstone equation, whose exact form still needs to be determined. We begin with the Bethe-Goldstone equation as formulated in Eqs. (2.1), (2.2) of Ref. 39. It is understood that \mathbf{p}, \mathbf{p}' are particle states and \mathbf{h}, \mathbf{h}' are hole states. Vectors \mathbf{k}, \mathbf{k}' can be either particle or hole states. Following Ref. 39, we introduce the pair wave function ψ in a

coordinate frame centered at the origin of the Fermi sea, given by the integral equation

$$\begin{aligned} \langle \mathbf{k}, \mathbf{k}' | \psi | \mathbf{h}, \mathbf{h}' \rangle &= \langle \mathbf{k}, \mathbf{k}' | \mathbf{h}, \mathbf{h}' \rangle \\ &- \bar{n}(k) \bar{n}(k') \frac{\langle \mathbf{k}, \mathbf{k}' | v \psi | \mathbf{h}, \mathbf{h}' \rangle}{t(k) + t(k') - t(h) - t(h')}. \end{aligned} \quad (2.30)$$

In making the connection to FHNC-EL, we should assume that the pair wave function is a function of the relative coordinate (or momentum), *i.e.*

$$\langle \mathbf{k}, \mathbf{k}' | \psi | \mathbf{h}, \mathbf{h}' \rangle = \frac{1}{N} \tilde{\psi}(q)$$

and set

$$\psi(r) = \sqrt{1 + \Gamma_{\text{dd}}(r)}. \quad (2.31)$$

Similarly, for local interactions, we should have

$$\langle \mathbf{k}, \mathbf{k}' | v \psi | \mathbf{h}, \mathbf{h}' \rangle = \frac{1}{N} [v(r) \psi(r)]^{\mathcal{F}}(q).$$

To ensure this, the energy denominator coefficient

$$\bar{n}(k) \bar{n}(k') \frac{\langle \mathbf{k}, \mathbf{k}' | v \psi | \mathbf{h}, \mathbf{h}' \rangle}{t(k) + t(k') - t(h) - t(h')}$$

must somehow be approximated by a function of momentum transfer q . This can be achieved by the averaging procedure (2.23) applied to the above energy denominator coefficient, to yield

$$2t_{\text{F}}(q) \lambda(q) [\psi(q) - \delta(q)] = -[v(r) \psi(r)]^{\mathcal{F}}(q). \quad (2.32)$$

Alternatively, and more in the spirit of Bethe and Goldstone, we write Eq. (2.30) as

$$\begin{aligned} [t(k) + t(k') - t(h) - t(h')] [\langle \mathbf{k}, \mathbf{k}' | \psi | \mathbf{h}, \mathbf{h}' \rangle - \langle \mathbf{k}, \mathbf{k}' | \mathbf{h}, \mathbf{h}' \rangle] \\ = -\bar{n}(k) \bar{n}(k') \langle \mathbf{k}, \mathbf{k}' | v \psi | \mathbf{h}, \mathbf{h}' \rangle. \end{aligned} \quad (2.33)$$

The approximation

$$t(|\mathbf{h} + \mathbf{q}|) - t(h) \approx \langle t(|\mathbf{h} + \mathbf{q}|) - t(h) \rangle (q) = t_{\text{F}}(q). \quad (2.34)$$

now gives Eq. (2.32) without the factor $\lambda(q)$ or, in coordinate space, we have

$$\begin{aligned} \left[-\frac{\hbar^2}{m} \nabla^2 + v(r) \right] \psi(r) \\ = \left[2t_{\text{F}}(q) (S_{\text{F}}(q) - 1) (\tilde{\psi}(q) - \delta(q)) \right]^{\mathcal{F}}(r). \end{aligned} \quad (2.35)$$

Eq. (2.35) is similar to, but not identical with, (2.21), which is obtained by the further assumption $\psi^2(r) - 1 \ll 1$. It therefore makes sense to assert $\psi(r) \approx \sqrt{1 + \Gamma_{\text{dd}}(r)}$. More importantly, the bare interaction of the Bethe-Goldstone equation is supplemented by the induced interaction. The identification between the two expressions (2.35) and (2.21) is not as precise as in the case of the ring diagrams, but note that FHNC-EL//0 contains more than just particle-particle ladders, also including particle-hole and hole-hole ladders [40].

D. Propagator corrections

Our analysis has so far addressed the question “what does it take to obtain a specific set of FHNC-EL diagrams from a corresponding set of Feynman diagrams ?” The analysis can be carried farther to other sets of diagrams. For example, the “cyclic chain” diagrams of the FHNC-EL method can be derived from the self-energy diagrams by the same localization procedure described above.

Once the approximations have been identified, it is also clear how to improve upon them: There is no reason to use the “collective approximation” (2.25) in both the frequency integrals (2.7) and the definition of the local effective interaction (2.10).

A second issue is then the generalization of the kinetic energy term $\left| \nabla \sqrt{1 + \Gamma_{\text{dd}}(\mathbf{r})} \right|^2$. To this end, we begin with the localized Bethe-Goldstone equation (2.32), where we supplement the bare interaction $v(r)$ by the induced interaction $w_I(r)$ and identify the pair wave function $\psi(r)$ with $\sqrt{1 + \Gamma_{\text{dd}}(r)}$. We then have two equations, namely (2.28), which can be written as

$$\widetilde{W}(q) = \widetilde{V}_{\text{p-h}}(q) + \widetilde{w}_I(q) = -t_{\text{F}}(q)\lambda(q)\widetilde{\Gamma}_{\text{dd}}(q), \quad (2.36)$$

along with the Bethe-Goldstone equation (2.32)

$$\begin{aligned} & 2 \left[t_{\text{F}}(q)\lambda(q) \left[\sqrt{1 + \Gamma_{\text{dd}}(r)} - 1 \right]^{\mathcal{F}}(q) \right]^{\mathcal{F}}(r) \\ & = -(v(r) + w_I(r))\sqrt{1 + \Gamma_{\text{dd}}(r)}. \end{aligned} \quad (2.37)$$

Multiplying the latter equation with $\sqrt{1 + \Gamma_{\text{dd}}(r)}$ and combining it with the former yields the expression

$$\begin{aligned}
V_{\text{p-h}}(r) &= [1 + \Gamma_{\text{dd}}(r)]v(r) + \Gamma_{\text{dd}}(r)w_{\text{I}}(r) \\
&\quad - \left[t_{\text{F}}(q)\lambda(q)\tilde{\Gamma}_{\text{dd}}(q) \right]^{\mathcal{F}}(r) + 2\sqrt{1 + \Gamma_{\text{dd}}(r)} \left[t_{\text{F}}(q)\lambda(q) \left[\sqrt{1 + \Gamma_{\text{dd}}(r)} - 1 \right]^{\mathcal{F}}(q) \right]^{\mathcal{F}}(r).
\end{aligned} \tag{2.38}$$

Note that if we have $t_{\text{F}}(q) = t(q)$ and $\lambda(q) = 1$, the terms on the second line combine to $\frac{\hbar^2}{m} \left| \nabla \sqrt{1 + \Gamma_{\text{dd}}(\mathbf{r})} \right|^2$. Since $S_{\text{F}}(q) = 1$ for $q > 2k_{\text{F}}$ and $\lambda(q) \rightarrow 1$ for large q , and never differs from 1 by more than 20 percent, the use of $\frac{\hbar^2}{m} \left| \nabla \sqrt{1 + \Gamma_{\text{dd}}(\mathbf{r})} \right|^2$ seems to be justified.

III. STATE-DEPENDENT CORRELATIONS

A. Operator structure

In this paper we focus on interactions of the so-called v_6 form, which in neutron matter involves only the first three operators spelled out in Eq. (1.2), *i.e.*

$$\hat{v}(r) = v_c(r)\mathbb{1} + v_\sigma(r)\boldsymbol{\sigma}_1 \cdot \boldsymbol{\sigma}_2 + v_S(r)S_{12}(\hat{\mathbf{r}}). \tag{3.1}$$

An alternative choice of the interaction operators is [25, 41]

$$\hat{v}(r) = v_c(r)\mathbb{1} + v_L(r)\hat{L}(\hat{\mathbf{r}}) + v_T(r)\hat{T}(\hat{\mathbf{r}}) \tag{3.2}$$

where

$$\hat{L}(\hat{\mathbf{r}}) \equiv (\boldsymbol{\sigma}_1 \cdot \hat{\mathbf{r}})(\boldsymbol{\sigma}_2 \cdot \hat{\mathbf{r}}), \quad \hat{T}(\hat{\mathbf{r}}) \equiv \boldsymbol{\sigma}_1 \cdot \boldsymbol{\sigma}_2 - (\boldsymbol{\sigma}_1 \cdot \hat{\mathbf{r}})(\boldsymbol{\sigma}_2 \cdot \hat{\mathbf{r}}) \tag{3.3}$$

are the ‘‘longitudinal’’ and ‘‘transverse’’ operators. These operators are amenable to summations of RPA-type diagrams because they have the features

$$\mathcal{T}r_{\boldsymbol{\sigma}_3} \hat{O}_i(1, 3)\hat{O}_j(3, 2) = 2\hat{O}_i(1, 2)\delta_{ij}, \quad \hat{O}_i(1, 2) \in \{\mathbb{1}, \hat{L}, \hat{T}\}. \tag{3.4}$$

A third useful set of operators are the projectors

$$\begin{aligned}
\hat{P}_s &= \frac{1}{4}(\mathbb{1} - \boldsymbol{\sigma}_1 \cdot \boldsymbol{\sigma}_2) \\
\hat{P}_{t+} &= \frac{1}{6}(3\mathbb{1} + \boldsymbol{\sigma}_1 \cdot \boldsymbol{\sigma}_2 + S_{12}(\hat{\mathbf{r}})) \\
\hat{P}_{t-} &= \frac{1}{12}(3\mathbb{1} + \boldsymbol{\sigma}_1 \cdot \boldsymbol{\sigma}_2 - 2S_{12}(\hat{\mathbf{r}})).
\end{aligned} \tag{3.5}$$

These satisfy the relations $\hat{P}_i(12)\hat{P}_j(12) = \hat{P}_i(12)\delta_{ij}$ and $\hat{P}_1 + \hat{P}_2 + \hat{P}_3 = \mathbb{1}$ and are therefore appropriate for solving the coordinate-space equations.

The three sets of operators are related through

$$\begin{aligned}
\begin{pmatrix} \mathbb{1} \\ \boldsymbol{\sigma}_1 \cdot \boldsymbol{\sigma}_2 \\ S_{12}(\hat{\mathbf{r}}) \end{pmatrix} &= \begin{pmatrix} 1 & 0 & 0 \\ 0 & 1 & 1 \\ 0 & 2 & -1 \end{pmatrix} \begin{pmatrix} \mathbb{1} \\ \hat{L} \\ \hat{T} \end{pmatrix} = \begin{pmatrix} 1 & 1 & 1 \\ -3 & 1 & 1 \\ 0 & 2 & -4 \end{pmatrix} \begin{pmatrix} \hat{P}_s \\ \hat{P}_{t+} \\ \hat{P}_{t-} \end{pmatrix}, \\
\begin{pmatrix} \mathbb{1} \\ \hat{L} \\ \hat{T} \end{pmatrix} &= \frac{1}{3} \begin{pmatrix} 3 & 0 & 0 \\ 0 & 1 & 1 \\ 0 & 2 & -1 \end{pmatrix} \begin{pmatrix} \mathbb{1} \\ \boldsymbol{\sigma}_1 \cdot \boldsymbol{\sigma}_2 \\ S_{12}(\hat{\mathbf{r}}) \end{pmatrix} = \begin{pmatrix} 1 & 1 & 1 \\ -1 & 1 & -1 \\ -2 & 0 & 2 \end{pmatrix} \begin{pmatrix} \hat{P}_s \\ \hat{P}_{t+} \\ \hat{P}_{t-} \end{pmatrix}, \\
\begin{pmatrix} \hat{P}_s \\ \hat{P}_{t+} \\ \hat{P}_{t-} \end{pmatrix} &= \frac{1}{4} \begin{pmatrix} 1 & -1 & -1 \\ 2 & 2 & 0 \\ 1 & -1 & 1 \end{pmatrix} \begin{pmatrix} \mathbb{1} \\ \hat{L} \\ \hat{T} \end{pmatrix} = \frac{1}{12} \begin{pmatrix} 3 & -3 & 0 \\ 6 & 2 & 2 \\ 3 & 1 & -2 \end{pmatrix} \begin{pmatrix} \mathbb{1} \\ \boldsymbol{\sigma}_1 \cdot \boldsymbol{\sigma}_2 \\ S_{12}(\hat{\mathbf{r}}) \end{pmatrix}.
\end{aligned} \tag{3.6}$$

B. Momentum space equation

Particle-hole matrix elements are best calculated in the operator basis $\{\mathbb{1}, \boldsymbol{\sigma}_1 \cdot \boldsymbol{\sigma}_2, S_{12}(\hat{\mathbf{r}})\}$, where for $O_1(1, 2)$ to $O_4(1, 2)$ we have

$$\begin{aligned}
&\langle \mathbf{h} + \mathbf{q}, \mathbf{h}' - \mathbf{q} | v_\alpha(1, 2) O_\alpha(1, 2) | \mathbf{h}, \mathbf{h}' \rangle \\
&= \frac{\rho}{N} \int d^3r v_\alpha(r) j_0(qr) O_\alpha(1, 2) \quad (1 \leq \alpha \leq 4)
\end{aligned} \tag{3.7}$$

whereas we have for tensor components we have

$$\begin{aligned}
&\langle \mathbf{h} + \mathbf{q}, \mathbf{h}' - \mathbf{q} |_\alpha(1, 2) O_\alpha(1, 2, \hat{\mathbf{r}}_{12}) | \mathbf{h}, \mathbf{h}' \rangle \\
&= -\frac{\rho}{N} \int d^3r v_\alpha(r) j_2(qr) O_\alpha(1, 2, \hat{\mathbf{q}}) \quad (5 \leq \alpha \leq 6).
\end{aligned} \tag{3.8}$$

Since there is no ambiguity, we will refer to both the j_0 Fourier transform and the $-j_2$ Fourier transform by the tilde symbol defined in Eq. (2.2).

The momentum-space equation (2.7) is best solved in the basis $\{\mathbb{1}, \hat{L}, \hat{T}\}$, where we simply get the response function and the static structure function in the above operator channels, *i.e.*

$$\chi_\alpha(q, \omega) = \frac{\chi_0(q, \omega)}{1 - \tilde{V}_{\text{p-h}}^{(\alpha)}(q) \chi_0(q, \omega)}, \tag{3.9}$$

$$S_\alpha(q) = -\int_0^\infty \frac{d\omega}{\pi} \text{Im} \chi_\alpha(q, \omega) \tag{3.10}$$

with $\alpha = 1, 3, 5..$ These equations are identical to those of Ref. 25 for bosons when the bosonic particle-hole propagator (2.8) is inserted, whereas they give Eq. (2.13) in the above three channels if the “collective” Lindhard function (2.25) is used. For the full Lindhard function, the integral must be carried out numerically. Likewise, both the energy-dependent and the energy-independent effective interactions $\widetilde{W}^{(\alpha)}(q, \omega)$ and $\widetilde{W}^{(\alpha)}(q)$, as well as the induced interaction (2.17), are obtained in this way, using Eq. (2.26). Of course, the tensor operator introduces an angular dependence.

C. Coordinate space equation

Owing to the projection property $\hat{P}_i(12)\hat{P}_j(12) = \hat{P}_i(12)\delta_{ij}$, the coordinate-space equations are best formulated in the projector basis $\{\hat{P}_s, \hat{P}_{t+}, \hat{P}_{t-}\}$. The only new aspect is that we must keep the angular dependence of the tensor correlations in the kinetic energy term $|\nabla\sqrt{1+\Gamma_{\text{dd}}(\mathbf{r})}|^2$. For its evaluation, let

$$\sum_{i=1}^3 (1 + \Gamma_{\text{dd}}^{(i)}(r))\hat{P}_i \equiv \left[\sum_{i=1}^3 f_i(r)\hat{P}_i \right]^2 = \sum_{i=1}^3 f_i^2(r)\hat{P}_i. \quad (3.11)$$

Then

$$\left| \nabla \sum_{i=1}^3 f_i(r)\hat{P}_i \right|^2 = \sum_{i=1}^3 \left| \frac{df_i(r)}{dr} \right|^2 \hat{P}_i - \frac{f_S^2(r)}{\hbar^2 r^2} |\mathbf{L}S_{12}(\hat{\mathbf{r}})|^2,$$

where $f_S(r) = (f_{t+}(r) - f_{t-}(r))/6$ is the component of $\hat{f}(\mathbf{r})$ in the tensor channel. The last term is simplified using

$$\begin{aligned} |\mathbf{L}S_{12}(\hat{\mathbf{r}})|^2 &= \frac{1}{2} [\mathbf{L}^2 S_{12}^2(\hat{\mathbf{r}}) - S_{12}(\hat{\mathbf{r}}) (\mathbf{L}^2 S_{12}(\hat{\mathbf{r}})) \\ &\quad - (\mathbf{L}^2 S_{12}(\hat{\mathbf{r}})) S_{12}(\hat{\mathbf{r}})]. \end{aligned} \quad (3.12)$$

Next, we invoke $\mathbf{L}^2 S_{12}(\hat{\mathbf{r}}) = 6\hbar^2 S_{12}(\hat{\mathbf{r}})$ and

$$S_{12}^2(\hat{\mathbf{r}}) = (2\hat{P}_{t+} - 4\hat{P}_{t-})^2 = 4\hat{P}_{t+} + 16\hat{P}_{t-}, \quad (3.13)$$

leading to

$$\begin{aligned} |\mathbf{L}S_{12}(\hat{\mathbf{r}})|^2 &= -6\hbar^2 S_{12}(\hat{\mathbf{r}}) - 6\hbar^2 S_{12}^2(\hat{\mathbf{r}}) \\ &= -36\hbar^2 \hat{P}_{t+} - 72\hbar^2 \hat{P}_{t-}. \end{aligned} \quad (3.14)$$

We arrive at

$$\left| \nabla \sum_{i=1}^3 f_i(r) P_i \right|^2 = \sum_{i=1}^3 \left| \frac{df_i(r)}{dr} \right|^2 \hat{P}_i + \frac{36}{r^2} f_S^2(r) \hat{P}_{t+} + \frac{72}{r^2} f_S^2(r) \hat{P}_{t-}. \quad (3.15)$$

Thereby, we have determined the structure of the particle-hole interaction in the three projector channels. We can now go back to the $\{\mathbb{1}, \hat{L}, \hat{T}\}$ basis and in momentum space and solve the equations iteratively.

D. Exchange corrections

Exchange diagrams have important consequences for the effective interactions, particularly in nucleonic systems. They must be included even at low densities to achieve consistency between the energetics and the quasiparticle interaction [29]. The simplest version of the FHNC hierarchy that corrects for this deficiency is FHNC//1, which includes the sum of the three exchange diagrams shown in Fig. 1.

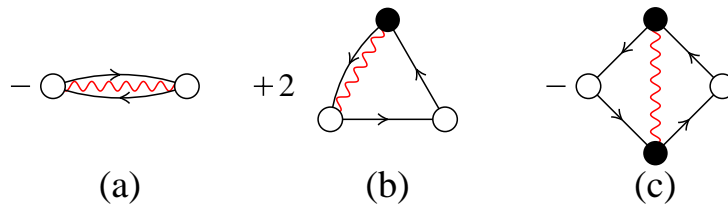


FIG. 1. The figure shows the diagrammatic representation of the lowest order exchange corrections $V_{ee}(r)$ and $X_{ee}(r)$. For the interaction correction $V_{ee}(r)$, the red wavy line is to be interpreted as the effective interaction $W(r_{ij})$. In the correlation correction $X_{ee}(r)$, the wavy red line represents the function $\Gamma_{dd}(r)$.

The relevant modification from the full FHNC-EL equations as formulated in Ref. 35 involves keeping only the exchange term $V_{ee}(k)$. The Euler equation becomes

$$S(q) = \frac{S_F(q) + \tilde{X}_{ee}(q)}{\sqrt{1 + \frac{2S_F^2(q)}{t(q)} \tilde{V}_{p-h}(q)}}. \quad (3.16)$$

where the particle-hole interaction is modified by

$$\tilde{V}_{\text{p-h}}(q) \rightarrow \tilde{V}_{\text{p-h}}(q) + \tilde{V}_{\text{ex}}(q), \quad \tilde{V}_{\text{ex}}(q) \equiv \frac{\tilde{V}_{\text{ee}}(q)}{S_{\text{F}}^2(q)} \quad (3.17)$$

and where $X_{\text{ee}}(r_{12})$ and $V_{\text{ee}}(r_{12})$ are given by the sum of the three diagrams shown in Fig. 1.

We have shown in Ref. 29 that naïve addition of exchange diagrams is problematic because it leads to an incorrect low-density limit of the pair correlations. We have rectified this situation by a slight modification of the Euler equation, namely

$$S(q) = S_{\text{F}}(q) \sqrt{\frac{1 + \frac{2S_{\text{F}}^2(q)}{t(q)}\tilde{V}_{\text{ex}}(q)}{1 + \frac{2S_{\text{F}}^2(q)}{t(q)}\tilde{V}_{\text{p-h}}(q)}}. \quad (3.18)$$

The square-root term in the numerator may be identified with a “collective RPA” expression for the exchange contribution to the static structure function (for state-independent interactions this is equal to the spin-structure function),

$$S_{\text{ex}}(q) = \frac{S_{\text{F}}(q)}{\sqrt{1 + \frac{2S_{\text{F}}^2(q)}{t(q)}\tilde{V}_{\text{ex}}(q)}}, \quad (3.19)$$

The expression (3.16) is then obtained by expanding $S_{\text{ex}}(q)$ to first order in the interactions and identifying

$$\tilde{X}_{\text{ee}}(q) \approx -\frac{S_{\text{F}}^3(q)}{t(q)}\tilde{V}_{\text{ee}}(q).$$

We have commented above on the fact that, with the qualification that the Jastrow-Feenberg wave function is not exact, the positivity of the term under the square root in the denominator is related to the stability against density fluctuations. Likewise, the positivity of the numerator is connected with the stability against spin-density fluctuations.

In time-dependent Hartree-Fock theory [42], the diagrams shown in Fig. 1 correspond to the particle-hole ladder diagrams, driven by the *exchange* term of the particle-hole interaction

$$W_{\text{ex}}(\mathbf{h}, \mathbf{h}'; \mathbf{q}) = \Omega \langle \mathbf{h} + \mathbf{q}, \mathbf{h}' - \mathbf{q} | W | \mathbf{h}', \mathbf{h} \rangle. \quad (3.20)$$

This non-local term supplements the RPA sum by the RPA-exchange (or particle-hole ladder) summation. The connection to the (local) FHNC expression (3.17) is made by realizing

that this expression is obtained from the exact expression (3.20) by exactly the same hole-state averaging process as was introduced in Eq. (2.23):

$$V_{\text{ex}}(q) = \frac{\tilde{V}_{\text{ee}}(q)}{S_{\text{F}}^2(q)} = \langle W_{\text{ex}}(\mathbf{h}, \mathbf{h}'; \mathbf{q}) \rangle (q). \quad (3.21)$$

For state-dependent correlations and interactions, we can simply go back to the definition (3.20) and interpret the interaction $W(r)$ as an operator of the form (3.1). The calculation for the central and spin components go exactly as before. The tensor component needs special treatment which will be outlined in the appendix .

E. Energy

In calculating the energy, we can again simply follow the analysis of Smith and Jackson, inserting exchange corrections where appropriate. We must keep in mind that there is no finite truncation scheme of the FHNC equations such that acceptable expressions for the pair distribution function and the static structure function are the Fourier transforms of each other. That is, having obtained an optimized static structure function $S(q)$, one must construct the pair distribution function $g(r)$ by appropriate combination of correlation diagrams and exchanges. In the case of state-independent correlations, the simplest expression for $g(r)$ is

$$g(r) = [1 + \Gamma_{\text{dd}}(r)] [g_{\text{F}}(r) + C(r)] \quad (3.22)$$

$$\tilde{C}(q) = [S_{\text{F}}^2(q) - 1] \tilde{\Gamma}_{\text{dd}}(q) + (\Delta\tilde{X}_{\text{ee}})(q). \quad (3.23)$$

where $g_{\text{F}}(r) = 1 - \frac{1}{2}\ell^2(rk_{\text{F}})$, with $\ell(x) = 3j_1(x)/x$ the pair distribution function of non-interacting fermions. In the FHNC//1 approximation, $S_{\text{F}}(q)$ is replaced by $S_{\text{F}}(q) + \tilde{X}_{\text{ee}}(q)$, and $(\Delta\tilde{X}_{\text{ee}})(q)$, which is represented by the sum of diagram (b) and (c) shown in Fig. 1 is added to $\tilde{C}(q)$. Summarizing, we obtain

$$\begin{aligned} \frac{E}{N} &= \frac{T_{\text{F}}}{N} + \frac{E_{\text{R}}}{N} + \frac{E_{\text{Q}}}{N}, \\ \frac{E_{\text{R}}}{N} &= \frac{\rho}{2} \int d^3r [g_{\text{F}}(r) + C(r)] \left[(1 + \Gamma_{\text{dd}}(r))v(r) \right. \\ &\quad \left. + \frac{\hbar^2}{m} \left| \nabla \sqrt{1 + \Gamma_{\text{dd}}(r)} \right|^2 \right], \end{aligned} \quad (3.24)$$

$$\frac{E_{\text{Q}}}{N} = \frac{1}{4} \int \frac{d^3q}{(2\pi)^3 \rho} t(q) \tilde{\Gamma}_{\text{dd}}^2(q) [S_{\text{F}}^2(q)/S(q) - 1], \quad (3.25)$$

where T_F is the kinetic energy of the non-interacting Fermi gas. In the state-dependent case, $g(r)$ becomes an operator in spin-space,

$$\begin{aligned}
\hat{g}(r) &= \left[1 + \Gamma_{\text{dd}}^{(s)}(r)\right] \left[1 + C_s(r) - \ell^2(rk_F)\right] \hat{P}_s \\
&+ \left[1 + \Gamma_{\text{dd}}^{(t+)}(r)\right] \left[1 + C_{t+}(r) + \ell^2(rk_F)\right] \hat{P}_{t+} \\
&+ \left[1 + \Gamma_{\text{dd}}^{(t-)}(r)\right] \left[1 + C_{t-}(r) + \ell^2(rk_F)\right] \hat{P}_{t-} \\
&\equiv g_s(r)\hat{P}_s + g_{t+}(r)\hat{P}_{t+}(r) + g_{t-}(r)\hat{P}_{t-}(r)
\end{aligned} \tag{3.26}$$

with which we obtain the potential energy

$$\begin{aligned}
\frac{\langle \hat{V} \rangle}{N} &= \frac{\rho}{2} \mathcal{T}r \int d^3r \hat{v}(r) \hat{g}(r) \\
&= \frac{\rho}{4} \int d^3r [v_s(r)g_s(r) + 2v_{t+}(r)g_{t+}(r) \\
&\quad + v_{t-}(r)g_{t-}(r)]
\end{aligned}$$

The kinetic energy term in Eq. (3.24) is generalized to state-dependent correlations in the same way, without the $[1 + \Gamma_{\text{dd}}^{(\alpha)}(r)]$ factors. Note, of course, that we need to keep the kinetic-energy correction spelled out in Eq. 3.15. Finally, the term E_Q is generalized to

$$\begin{aligned}
\frac{E_Q}{N} &= \frac{1}{4} \int \frac{d^3q}{(2\pi)^3 \rho} t(q) \sum_{\alpha} (\tilde{\Gamma}_{\text{dd}}^{(\alpha)})^2(q) [S_F^2(q)/S_{\alpha}(q) - 1] \times \\
&\quad \times \mathcal{T}r O_{\alpha}^2(1, 2) \quad O_{\alpha} \in \{\hat{1}, \hat{L}, \hat{T}\}.
\end{aligned} \tag{3.27}$$

IV. RESULTS

In applying the EL-FHNC procedures established in preceding sections, we have chosen as inputs the v_6 truncation of the Reid interaction as formulated in Ref. 3 and the Argonne v'_6 interaction [4]. For each of these interactions, we have performed a sequence of computations. In terms of correlation operators $\Gamma_{\text{dd}}^{(\alpha)}(r)$, (i) keeping only central components, (ii) including both central and spin operators, and (iii) supplementing the latter with tensor operators, in each case omitting or keeping the exchange diagrams described in Section III D. Additionally, we have used the ‘‘collective approximation’’ (2.25) as well as the exact Lindhard function in both the calculation of $S(q)$ by means of Eq. (2.7) and the calculation of the effective interaction through Eq. (2.26). As is usual in FHNC notation, we designate the level at which exchange diagrams are included by //n, e.g., //0 means no exchanges are included,

while //1 means that we keep the one-line diagrams $X_{ee}^{(1)}(r)$ and $V_{ee}^{(1)}(r)$. Calculations using the “collective approximation” will be referred to as “FHNC” and those containing the exact particle-hole propagator, as “parquet”.

A. Energetics

We shall refrain here from showing the large array of results obtained in the FHNC and parquet versions of the theory and focus on the most telling implementations. Our calculations have been extended to much lower densities than is usually done [26], since the regime of very low density has been of recent interest due to the expectation there is some fundamental similarity between low-density neutron matter and the unitary gas. Among other significant features, the superfluid gap at low densities is close to 0.5 times the Fermi energy [43–45]. However, we did not go quite as low in density as in our previous work, since good resolution in both coordinate and momentum space would require a much larger mesh.

The first quantity of interest is, of course, the energy per particle, with results exhibited in Fig. 2. Shown there are only the calculations containing exchange diagrams and the full particle-hole propagator, the plots for other calculations being omitted for clarity.

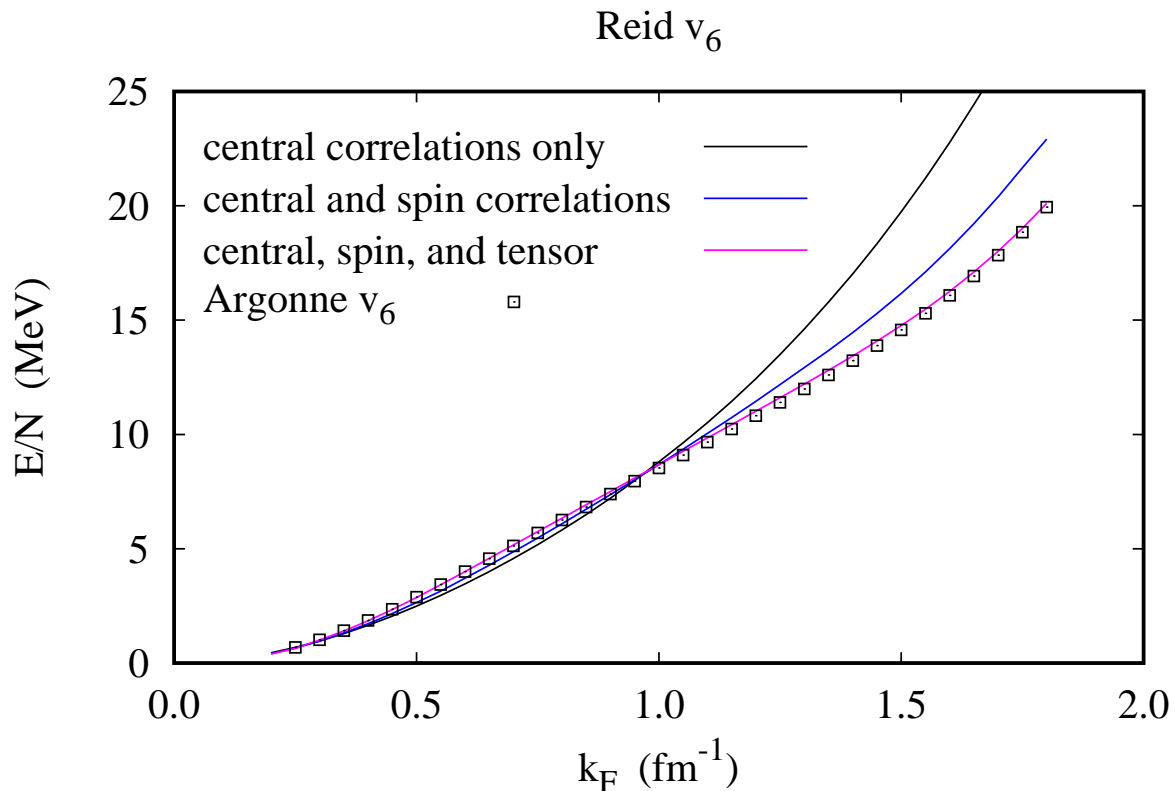


FIG. 2. (color online) The neutron-matter equation of state for the Reid v_6 potential is plotted versus Fermi wave number k_F in three approximations: (i) accounting only for central correlations (black line), (ii) including both spin and central correlations (blue line), and (iii) further introducing tensor correlations (magenta line). Also shown, for the third case of central, spin, and tensor correlations, are results for the Argonne v_6 potential (boxes).

We observe that the equations of state begin to differ visibly beyond $k_F = 1\text{fm}^{-1}$, we note, of course, that at that density the FHNC//0 and FHNC//1 approximations deviate from a full FHNC-EL calculation by about the same amount, see Fig. 3 and Fig. 1 of Ref. 45. In fact, in view of the difference in the correlation functions found in different approximations to be discussed below we find the agreement between different calculations rather remarkable. We also direct the attention to the fact that the results for the Argonne potential are rather close to those of the Reid interaction.

As stated above, we keep the comparison with earlier calculations to a minimum because extensive work is available [26]. Fig. 3 gives an update for two versions of the Argonne potential [4] including the calculations of this work, the state-independent full FHNC-EL

calculations of Ref. 45, the Brueckner-Hartree-Fock calculations of Baldo *et al.*, and the auxiliary-field diffusion Monte Carlo (AFDMC) method [46].

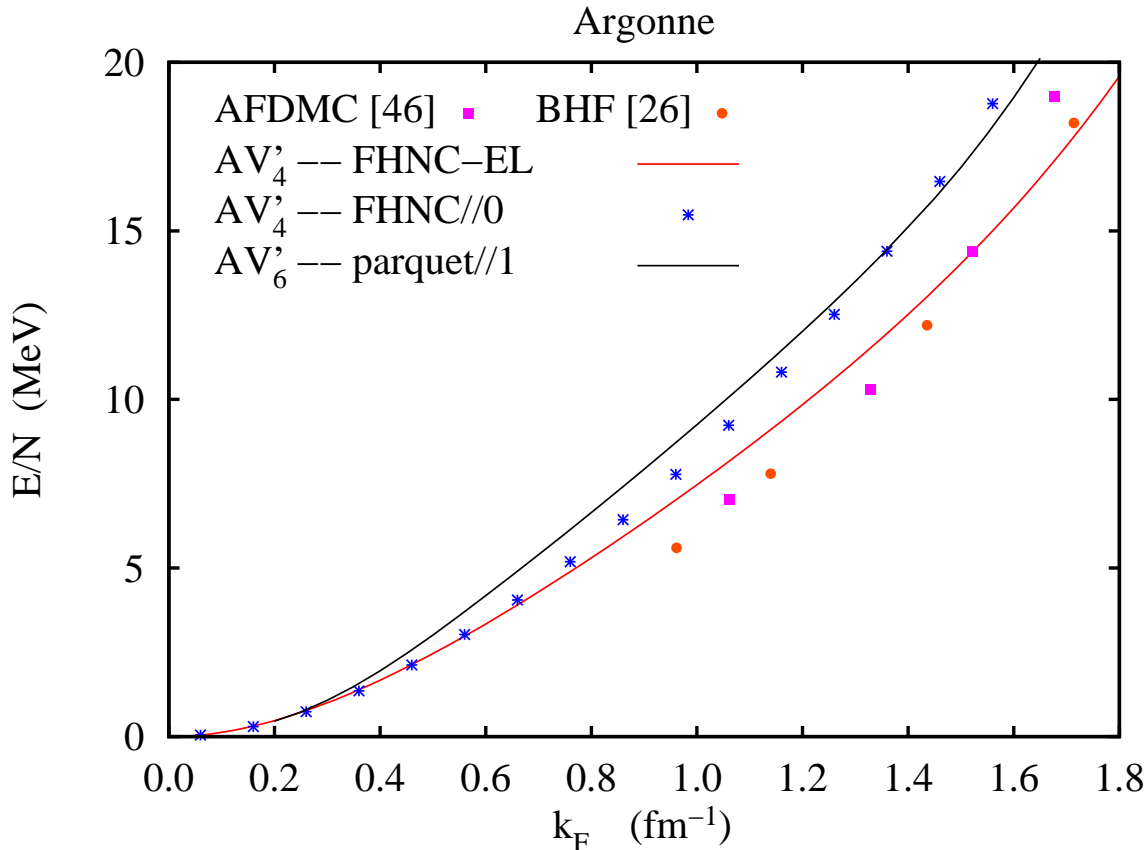


FIG. 3. (color online) The figure shows a comparison of neutron matter equation of state for the Argonne v'_4 and v'_6 interactions for the state-independent FHNC-EL and FHNC//0 calculations of Ref. 45, the present work, as well as from the auxiliary-field diffusion Monte Carlo (AFDMC) method [46] for the Argonne v_{18} interaction and from a Brueckner-Hartree-Fock calculation [26] for the Argonne v'_4 potential.

The close similarity of the energetics exhibited in Fig. 2 for the three quite different calculations is, however, by no means an indication that central correlations are sufficient for a description of this system, as was demonstrated in another sequence of calculations. Fig. 4 shows the bare interactions in the three projector channels \hat{P}_s , \hat{P}_{t+} , and \hat{P}_{t-} , along with the dynamic correlation functions $1 + \Gamma_{\text{dd}}^{(\alpha)}(r)$ in these channels. Obviously the interactions are very different; for example, recall that the S -wave interaction has a scattering length of $a_0 \approx -18.7$ fm [47], *i.e.* it is close to developing a bound state. Correspondingly, the correlation develops a strong peak roughly at the location of the interaction minimum. The

two triplet channels are much less attractive; in fact the $t+$ channels is repulsive, hence the particles tend to be pushed apart.

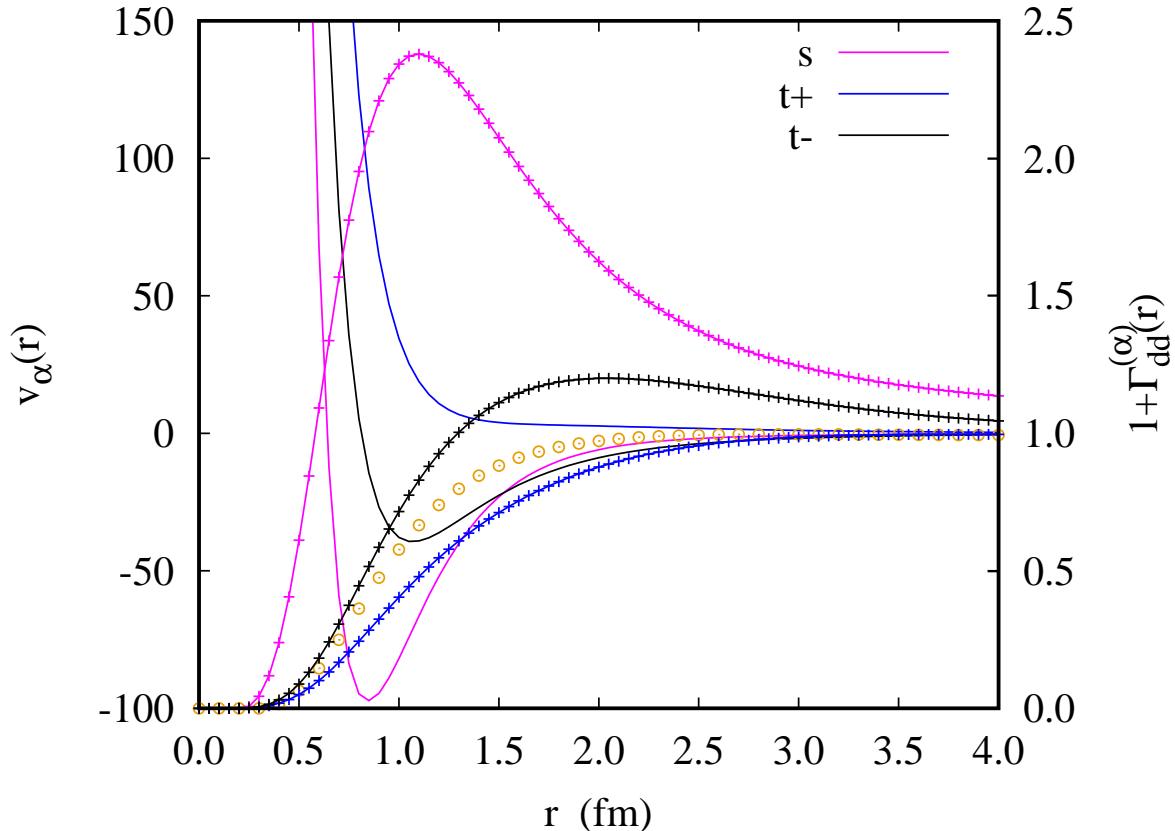


FIG. 4. (color online) Plots, versus radial separation r , of the components of the Reid v_6 interaction in spin-triplet states and of the corresponding projectors \hat{P}_s , \hat{P}_{t+} , and \hat{P}_{t-} (magenta, blue, and black), together with the dynamic correlation functions $1 + \Gamma_{\text{dd}}^{(\alpha)}(r)$ in these channels (same colors, lines with “+” markers), all at Fermi wave number $k_{\text{F}} = 1 \text{ fm}^{-1}$. Also shown is the correlation function $1 + \Gamma_{\text{dd}}(r)$ for state-independent correlations (yellow circles).

We conclude this section with a brief comparison with other many-body approaches; a very extensive comparison of numerical data from different approaches may be found in Ref. 26.

Variational and perturbative calculations are often referred to as complimentary approaches. We feel that this view is somewhat oversimplified: It was already observed by Sim *et al.* [33], and re-iterated by Jackson *et al.* [15–17] that the boson Bethe-Goldstone equation is indeed a proper subset of the calculation within the optimized HNC scheme. We have clarified above and in Ref. 29 to what extent the same is true for fermions. We have

come to the conclusion that the only additional postulate is that the pair wave function is a function of the interparticle distance; see section II C 3. In other words, for fermions the Brueckner-Hartree-Fock (BHF) theory is also a proper subset of FHNC-EL. The essential difference is that in conventional (BHF), *ad-hoc* constraints must be introduced to prevent the pair wave function from becoming unphysically long ranged [48]. Exactly the same is true when a variational theory is truncated at low order: The Euler-equation in 2-body approximation has unphysically long-ranged solutions that must be somehow tamed; this is done, for example, by the so-called “low-order constrained variational (LOCV) method.” In the FHNC-EL scheme, the “induced interaction” $w_I(r)$ makes sure that the long-ranged behavior of the correlations is physically reasonable; artificially imposed constraints are therefore unnecessary.

B. Correlation and Distribution functions

Two questions are addressed in this subsection: The first is what it takes to have a reliable prediction for the distribution and structure functions, and the second, once that is determined, how physical quantities of interest depend on density and specific features of the interaction.

We have partly addressed the first issue already in the preceding subsection, where we have shown that simple state-independent correlations can reproduce the energetics with reasonable accuracy, but they give no reliable prediction for the dynamic correlations. The other question is concerned with the importance of exchange diagrams and propagator corrections. We address this question partly in Fig. 5 and Fig. 6, where we show the dynamic correlation function and the pair distribution function in the singlet channel in four different approximations: without and with the exchange contribution and propagator corrections (labeled FHNC//0 and FHNC//1), as well as with propagator corrections (labeled parquet//0 and parquet//1). Evidently, all of these corrections have little consequence for the direct dynamic correlations.

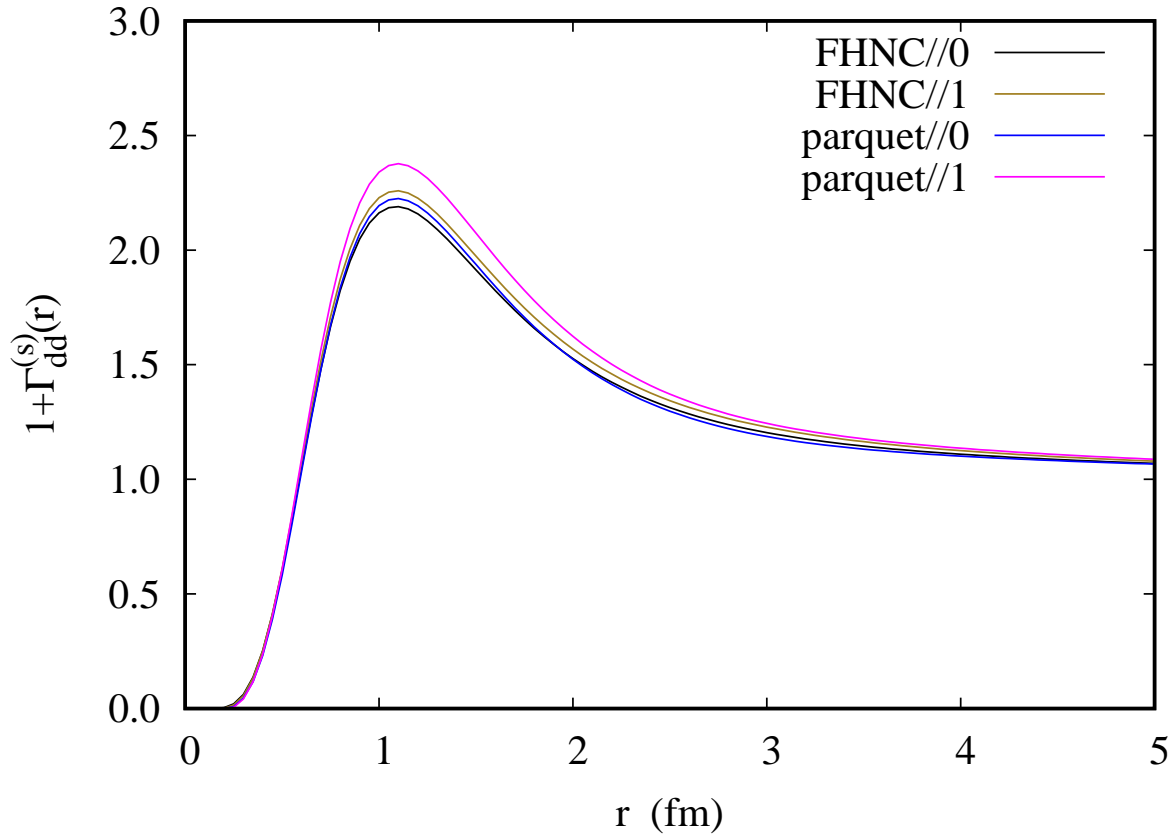


FIG. 5. (color online) Plots, at Fermi wave number $k_F = 1 \text{ fm}^{-1}$, of the spin-singlet dynamic correlation function $1 + \Gamma_{\text{dd}}^{(s)}(r)$ versus radius r , as obtained in the four different approximations explained in the text.

The situation changes remarkably for the pair distribution function (Fig. 6), where we see that exchanges have a rather drastic effect. We hasten to explain that this is exclusively due to the term $(\Delta \tilde{X}_{ee})(q)$ spelled out in Eq. (3.23); the replacement $S_F(q) \rightarrow S_F(q) + (\Delta \tilde{X}_{ee})(q)$ has a negligible effect. It was observed a long time ago that the sum of the three diagrams shown in Fig. 1 is much smaller than the three individual terms [49]; the fact that the individual terms are quite large is peculiar to the present situation. These terms are relatively small in ^3He and low-density gases.

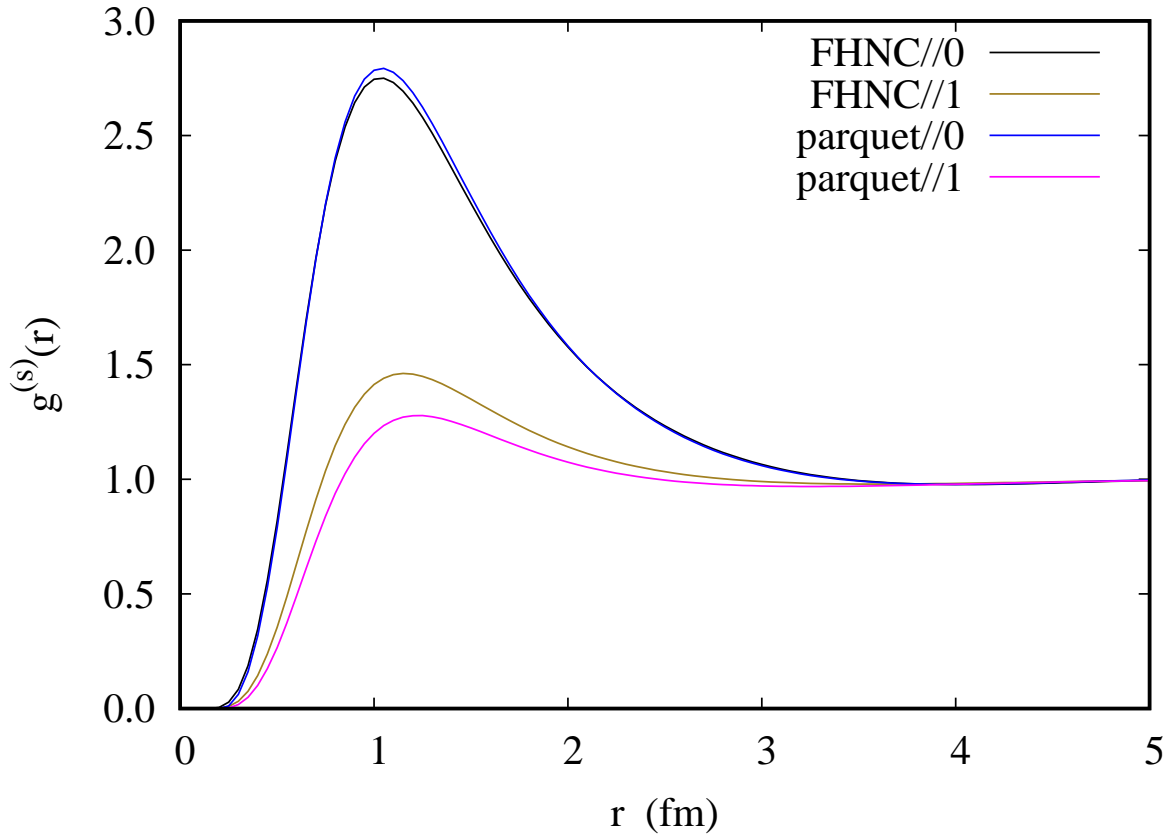


FIG. 6. (color online) This figure shows, at $k_F = 1 \text{ fm}^{-1}$, the spin-singlet pair distribution function in the four different approximations as explained in the text.

Let us finally turn to the density dependence of the correlations. We have already pointed out that the s -channel is close to forming a bound state; accordingly, we find that the s -projection of the correlation function develops a strong nearest-neighbor peak as the density decreases. With increasing density, this peak is suppressed, evidently by both the Pauli principle and the induced interaction $w_1(r)$.

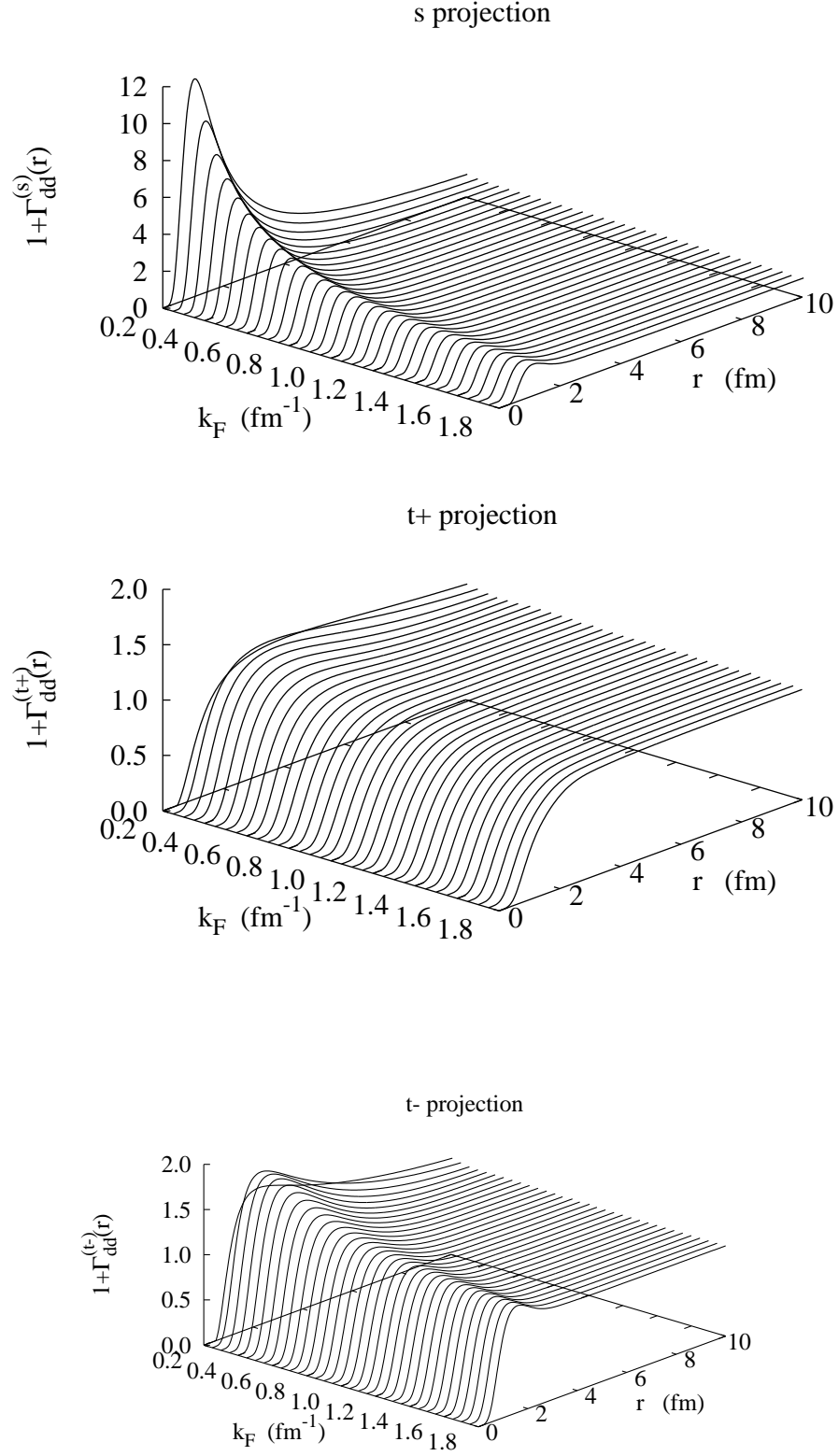


FIG. 7. The figure shows the density dependence of the dynamic correlation functions $1 + \Gamma_{\text{dd}}^{(\alpha)}(r)$ in the three spin-projector channels s (Fig. 7(a)), $t+$ (Fig. 7(b)), and $t-$ (Fig. 7(c)),

C. Effective interactions

Effective interactions are perhaps more relevant than ground state properties because they determine quantities like the response [50] and pairing properties [51] that are directly observable. We address here again the same two questions that we have posed above: What is an acceptable computational procedure to determine these interactions, and how do they depend on external parameters like the density ?

The most important input for linear response theory and, hence for the calculation of the dynamic structure function, is the particle-hole interaction. The long-wavelength limit of the particle-hole interaction is related to the hydrodynamic speed of sound by

$$mc^2 = \frac{d}{d\rho} \rho^2 \frac{dE}{d\rho N}. \quad (4.1)$$

In a Fermi fluid, we also have Pauli repulsion, reflected in the relation

$$mc^2 = mc_F^{*2} + \tilde{V}_{p-h}(0+) \equiv mc_F^{*2}(1 + F_0^S), \quad (4.2)$$

where $c_F^* = \sqrt{\frac{\hbar^2 k_F^2}{3mm^*}}$ is the speed of sound of the non-interacting Fermi gas with the effective mass m^* , and F_0^S is Landau's Fermi liquid parameter. Requiring a positive compressibility leads to Landau's stability condition $F_0^S > -1$.

The relationships (4.1) and (4.2) normally give identical predictions only in an exact theory [52, 53]; good agreement is typically reached only at very low densities. The reason for that is the very simple fact that the convergence of cluster expansions for the Fermi-Liquid parameters is intrinsically worse than that for the energy [52]: The contribution to any n -body diagram to the energy is multiplied by roughly a factor n^2 in an equivalent expansion of the incompressibility from Eq. (4.1). Even in the much simpler system ${}^4\text{He}$, where four- and five-body elementary diagrams and three-body correlations are routinely included, the two expressions (4.1) and (4.2) can differ by up to a factor of 2 [54].

The situation is even more complicated in Fermi systems due to the multitude of exchange diagrams, of which we kept only the simplest. Hence, one can expect good agreement only at very low densities [29], but not at the densities considered here.

Fig. 8 compares the results from Eqs. (4.1) and (4.2) for the Reid v_6 interaction and the parquet//1 calculation including tensor correlations, shown as the magenta curve in Fig. 2. The derivative (4.1) was calculated by finite differences, to eliminate numerical noise mc^2 has been fitted by a third-order polynomial.

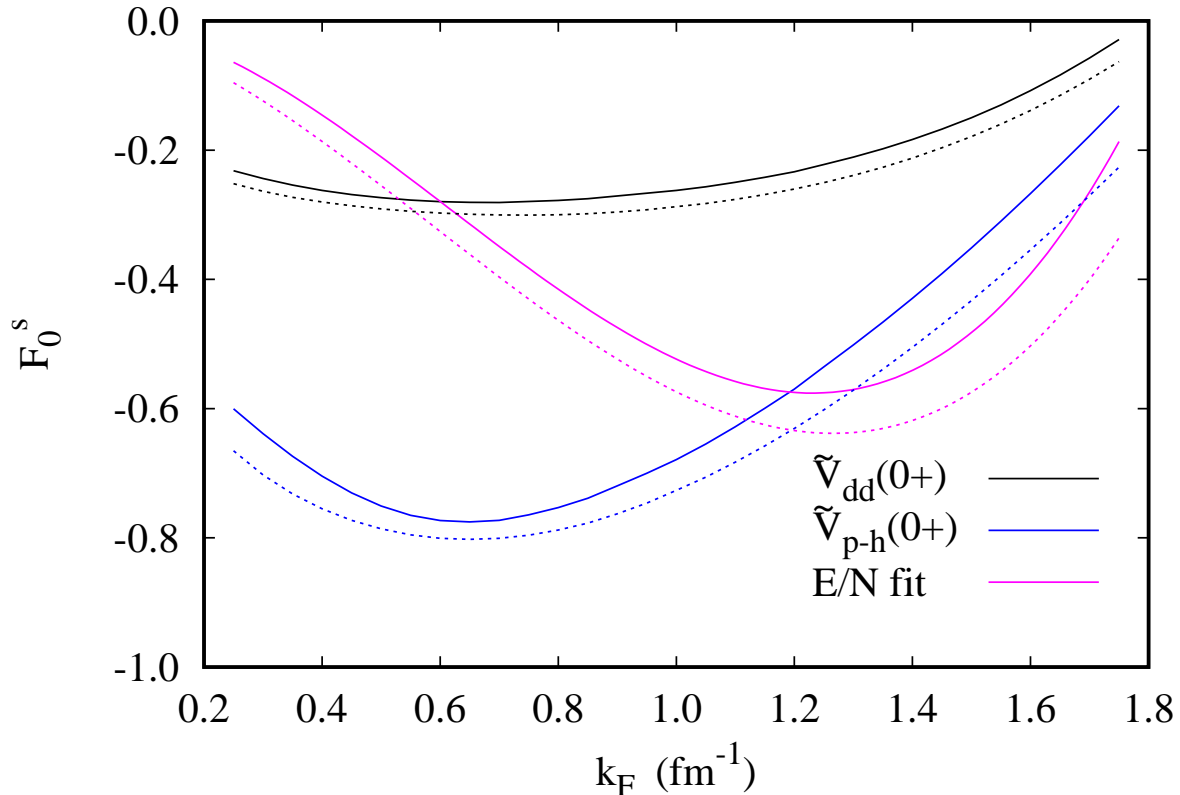


FIG. 8. (color online) This figure shows the density dependence of the Fermi liquid parameter F_0^s , as obtained from the speed of sound via the derivative (4.1) (magenta line) and from the long-wavelength limit (4.2) of the microscopic particle-hole interaction. The black curve contains only the “direct” part (2.15), while the blue line contains both direct and exchange parts. The solid lines show parquet//1 results, whereas the dashed lines show results from FHNC//1.

To connect microscopic and hydrodynamic speeds of sound we have used an effective mass ratio $m^*/m = 1$, which seems to be justified by our results from Ref. 29. A number of conclusions can be drawn from Fig. 8. The “direct” part is somewhat improved compared with the calculation based on state-independent interactions, where the F_0^s came out positive (*cf.* Fig. 9 of Ref. 29). One would have expected that F_0^s goes to zero linearly as $k_F \rightarrow 0$; this appears to happen only at much lower densities. The underlying cause seems to be the strong density dependence of the singlet correlation functions shown in Fig. 7(a). The state-independent calculation of Ref. 29 does not have this feature – linear behavior can be observed up to $k_F \lesssim 0.4 \text{ fm}^{-1}$. We also find that the contribution from exchange diagrams is quite substantial. We attribute the remaining difference partly to higher-order exchange

diagrams, but also to the omission of “elementary” diagrams.

In Fig. 9 we turn to the reliability of the derived particle-hole interaction in successive approximations, *i.e.*, using central correlations, both central and spin-dependent correlations, and finally adding tensor correlations. Evidently, central correlations cannot give a valid prediction of the particle-hole interaction. Important corrections come from the contribution from exchange diagrams, $\tilde{V}_{\text{ex}}(k)$. This is to be expected and is consistent with our findings from Fig. 8 and Ref. 29. Tensor correlations introduce some attraction at long wavelengths, but have minimal impact on the effective interaction in the central channel.

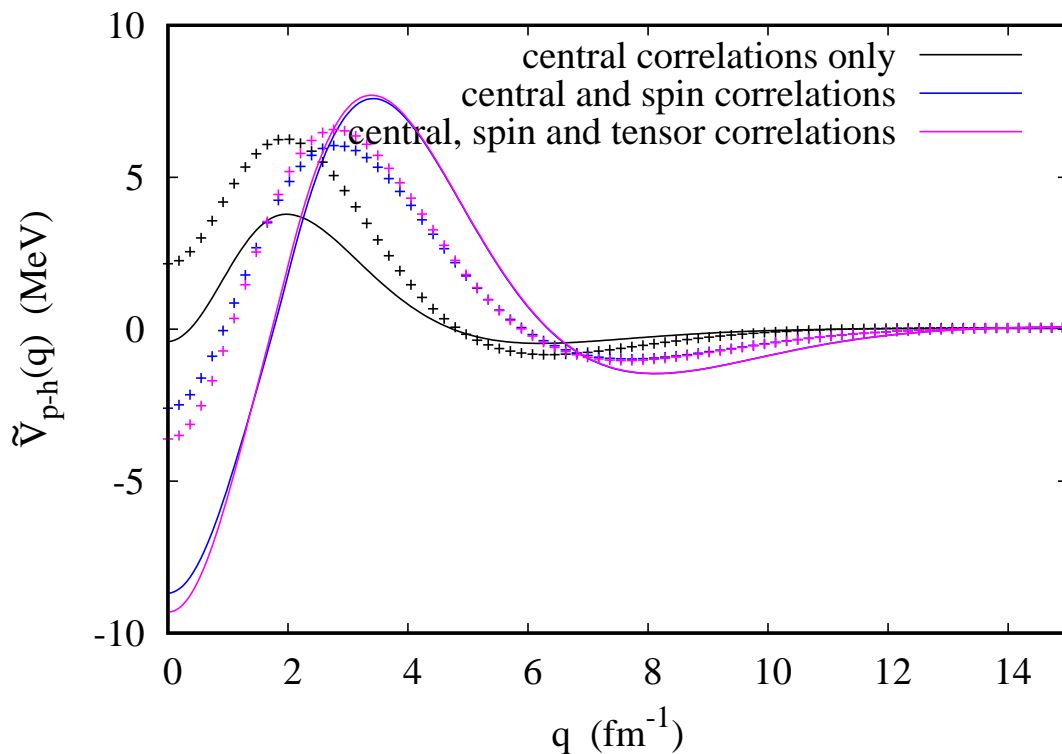


FIG. 9. (color online) For $k_F = 1 \text{ fm}^{-1}$, this figure depicts the central channel of the particle-hole interaction $\tilde{V}_{\text{p-h}}(q)$ (Eq. (3.17)), based on (i) state-independent correlation functions (solid black line), (ii) spin-dependent correlations (blue line), and (iii) spin and tensor correlations (magenta line). Also shown is the direct part, given by Eq. (2.15), in the three approximations (+ symbols, same color).

An overview of the density dependence of the effective interactions in the three channels $\{\mathbb{1}, \hat{L}, \hat{T}\}$ is provided in Figs. 10. We emphasize, as discussed above, that only the central

channel is attractive, whereas both the longitudinal and transverse channel interactions are repulsive.

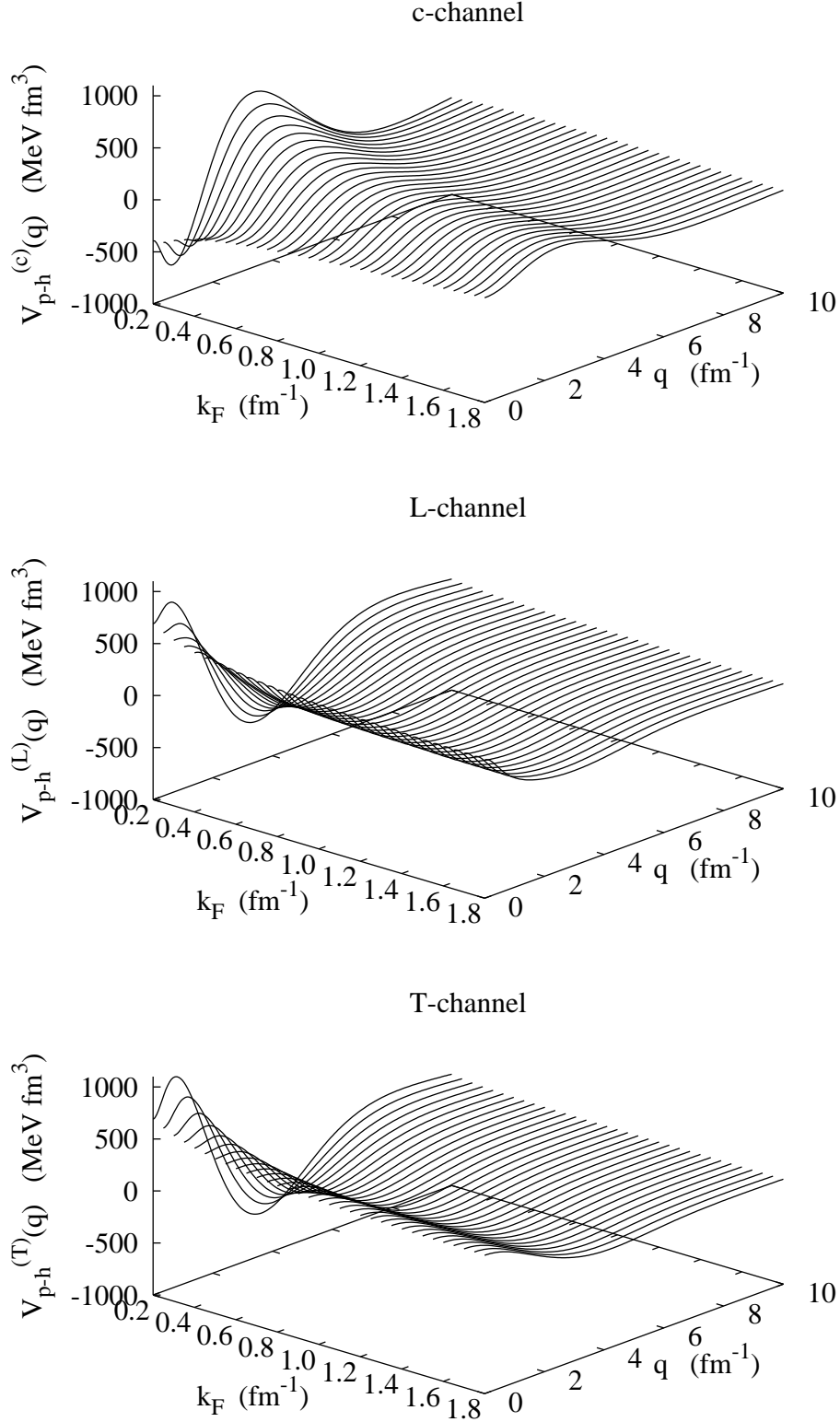


FIG. 10. This figure demonstrates the density dependence of the particle-hole interaction $V_{p-h}^{(\alpha)}(q)$ in the three operator channels $\alpha = c$ (Fig. 10(a)), L (Fig. 10(b)), and T (Fig. 10(c)). Note that we show here $V_{p-h}^{(\alpha)}(q) = \tilde{V}_{p-h}^{(\alpha)}(q)/\rho$ in order to make the low-density behavior visible.

Generally, we have not found a significant change of our results caused by propagator corrections. Approximating the response function by a “collective” version can be expected to be a good approximation only if the system has a strong collective mode. This is the case for both the transverse and the longitudinal channels, where the interactions are repulsive. The most likely case where a correction could be found would be the singlet channel because there we have a negative F_0^s , which means that the zero-sound mode is Landau damped. We found, nevertheless, that the collective approximation (2.25) in the RPA expression (2.7) is very good, being most important when the system approaches the stability limit $F_0^s \rightarrow -1$.

The particle-hole interactions are necessary input for the calculation of excitations, whereas the other effective interactions, $\hat{W}_\alpha(r)$, are necessary for the calculation of pairing properties [29, 55, 56]. The latter differ from the particle-hole interactions only by the induced interaction $w_1(r)$; see Eq. (2.11). In the present cases, we found that these corrections are rather small and it would offer little further insight to show them.

V. SUMMARY

In this paper, we have taken up work by Smith and Jackson [25] and generalized it to Fermi systems. In doing so, we have relied heavily on what is known from the optimized variational (F)HNC method and made use of the fact that the parquet equations of Ref. 25 could also be obtained from the bosonic version of the (F)HNC equations of Fantoni and Rosati [18]. In that way, and also by comparison with the state-independent Jastrow-Feenberg case [29], we have been able to identify the localization procedures leading from the general parquet equations to the “local” ones. In the boson case, there was just one such procedure, namely the approximation of the generally energy-dependent induced interaction by an energy-independent form (2.10), which holds for both bosons and fermions. This was already recognized in Ref. 57. In the case of fermions, there is an additional localization procedure, which leads to correlation functions depending only on the interparticle distance (see Eq. (2.23)), which turns the pair wave function of the Bethe-Goldstone equation into a function of the interparticle distance.

Our procedure goes beyond the so-called “FHNC-SOC” (single-operator-chain) approximation in the following sense. The SOC approximation calculates only the operator-dependent chain diagrams, the correlation functions in these channels commonly being ob-

tained by the LOCV procedure. In that sense, the SOC approximation may be understood as an RPA with an effective interaction [58]. We also sum these chain diagrams, but our correlation functions are determined, in all operator channels, by the localized Bethe-Goldstone equation. Moreover, the “induced interactions” also have the full operator structure.

The present implementation of the parquet theory does not solve the notorious problem of the commutator diagrams. Model studies for a fictitious system of bosons with spins [21] have indicated that they can be very important if the interactions in spin-singlet and spin-triplet cases are very different, which is indeed the case here, as indicated in Figs. 7. However, comparison with parquet theory should offer a much more elegant solution of the problem of commutators than carrying out the symmetrization operators for a variational wave function of the form (1.6). The next step in implementing the parquet strategy is to generalize the Bethe-Goldstone equation to include all time-orderings of the induced interaction $w_1(r)$ in the summation of ladder diagrams, thereby superseding the Bethe-Goldstone equation. Work in this direction is in progress.

Appendix: Calculation of exchange diagrams

The easiest way to calculate the exchange corrections is to begin with Eq. (3.20):

$$V_{\text{ex}}(q) = \langle W_{\text{ex}}(\mathbf{h}, \mathbf{h}', \mathbf{q}) \rangle . \quad (\text{A.1})$$

The input is normally a coordinate-space representation of $W(1, 2)$; in other words the effective interaction has the form

$$\hat{W}(1, 2) = W_0(r)\hat{P}_s + W_+(r)\hat{P}_{t+} + W_-(r)\hat{P}_{t-} . \quad (\text{A.2})$$

The calculation of the central has been outlined in Ref. 49; spin-correlations are dealt with in exactly the same way. The matrix elements of the tensor operator must be calculated independently. A working formula for these exchange diagrams is

$$\begin{aligned} \tilde{V}_{\text{ee}}(k) = -\frac{\rho}{\nu} \int d^3r \mathcal{W}(\mathbf{r}) & \left[\ell^2(rk_{\text{F}})j_0(rk) - \right. \\ & \left. \ell(rk_{\text{F}})(I(\mathbf{k}; \mathbf{r}) + I^*(\mathbf{k}; \mathbf{r})) + I(\mathbf{k}; \mathbf{r})I^*(\mathbf{k}; \mathbf{r}) \right] . \end{aligned} \quad (\text{A.3})$$

Here $I(\mathbf{k}; \mathbf{r})$ is conveniently calculated by an expansion in spherical harmonics,

$$\begin{aligned} I(\mathbf{k}; \mathbf{r}) &= \frac{3}{4\pi k_{\text{F}}^3} \int d^3k' e^{i\mathbf{k}' \cdot \mathbf{r}} n(k') n(|\mathbf{k} - \mathbf{k}'|) \\ &= \sum_{\ell} (2\ell + 1) i^{\ell} P_{\ell}(\cos(\hat{\mathbf{k}} \cdot \hat{\mathbf{r}})) c_{\ell}(k, r) \end{aligned} \quad (\text{A.4})$$

with

$$c_{\ell}(k, r) = \frac{3}{2k_{\text{F}}^3} \int_0^{k_{\text{F}}} dp p^2 j_{\ell}(rp) \int_{x_L}^1 dx P_{\ell}(x) , \quad (\text{A.5})$$

where

$$x_L = \begin{cases} 1 & \text{if } |p - k| > k_{\text{F}} \\ -1 & \text{if } p + k < k_{\text{F}} \\ \frac{p^2 + k^2 - k_{\text{F}}^2}{2pk} & \text{otherwise .} \end{cases} \quad (\text{A.6})$$

For central forces this procedure gives

$$\begin{aligned} \tilde{V}_{\text{ee}}(k) = -\rho \int d^3r \mathcal{W}(r) & \left[\ell^2(rk_{\text{F}})j_0(rk) - 2\ell(rk_{\text{F}})c_0(k; r) \right. \\ & \left. + \sum_{\ell=0}^{\infty} (2\ell + 1) c_{\ell}^2(k; r) \right] . \end{aligned} \quad (\text{A.7})$$

We have verified in Ref. 49 that keeping $c_0(k, r)$ and $c_1(k, r)$ is generally sufficient.

For the tensor force, we obtain

$$\begin{aligned} \tilde{V}_{S,ij}(\mathbf{k}) = & -\rho \int d^3r \mathcal{W}_S(r) (3\hat{x}_i\hat{x}_j - \delta_{ij}) \left[\ell^2(rk_F) e^{i\mathbf{k}\cdot\mathbf{r}} \right. \\ & \left. - \ell(rk_F) (I(\mathbf{k}; \mathbf{r}) + I^*(\mathbf{k}; \mathbf{r})) + I(\mathbf{k}; \mathbf{r}) I^*(\mathbf{k}; \mathbf{r}) \right]. \end{aligned}$$

The first term is just the j_2 Fourier transform. The other two terms can be calculated by expansion in spherical harmonics. The contributions from the $c_0(k, r)$ terms are zero due to the angle integration. The only term that survives is the c_1 contribution from the last term, which reads

$$\begin{aligned} & -9\rho \int d^3r \mathcal{W}_S(r) c_1^2(k, r) \sum_{ij} (3\hat{x}_i\hat{x}_j - \delta_{ij}) z^2 \sigma_i \sigma_j \\ & = -\frac{18}{15} \rho \int d^3r \mathcal{W}_S(r) c_1^2(k, r) (2\sigma_z \sigma_z - \sigma_z \sigma_x - \sigma_y \sigma_y) \\ & = -\frac{6}{5} \rho \int d^3r \mathcal{W}_S(r) c_1^2(k, r) S_{12}(\hat{\mathbf{k}}). \end{aligned} \tag{A.8}$$

If we keep only $c_0(k, r)$ and $c_1(k, r)$ we arrive at

$$\tilde{V}_{\text{ex}}[W_S] = \rho \int d^3r \mathcal{W}_S(r) \left[\ell^2(rk_F) j_2(kr) - \frac{6}{5} c_1^2(k, r) \right]. \tag{A.9}$$

ACKNOWLEDGMENTS

This work was supported, in part, by the the College of Arts and Sciences of the University at Buffalo, SUNY. Encouragement for this work was derived from a workshop on *Nuclear Many-Body Theories: Beyond the mean field approaches* at the Asia Pacific Center for Theoretical Physics in Pohang, South Korea, in July 2019. We thank J. W. Clark for numerous comments and suggestions on this manuscript. One of us (JW) thanks the Austrian Marshall Plan Foundation for support during the summer 2018 and Robert Zillich for discussions.

-
- [1] R. V. Reid, Jr., *Ann. Phys. (NY)* **50**, 411 (1968).
- [2] H. A. Bethe and M. B. Johnson, *Nucl. Phys. A* **230**, 1 (1974).
- [3] B. D. Day, *Phys. Rev. C* **24**, 1203 (1981).
- [4] R. B. Wiringa, V. G. J. Stoks, and R. Schiavilla, *Phys. Rev. C* **51**, 38 (1995).
- [5] R. B. Wiringa, R. A. Smith, and T. L. Ainsworth, *Phys. Rev. C* **29**, 1207 (1984).
- [6] E. Feenberg, *Theory of Quantum Fluids* (Academic, New York, 1969).
- [7] M. Kalos, D. Levesque, and L. Verlet, *Phys. Rev. A* **9**, 2178 (1974).
- [8] D. M. Ceperley, *Phys. Rev. B* **18**, 3126 (1978).
- [9] D. M. Ceperley, *Rev. Mod. Phys.* **67**, 279 (1995).
- [10] J. Boronat, in *Microscopic Approaches to Quantum Liquids in Confined Geometries*, edited by E. Krotscheck and J. Navarro (World Scientific, Singapore, 2002) pp. 21–90.
- [11] T. Morita, *Progr. Theor. Phys.* **20**, 920 (1958).
- [12] J. M. J. van Leeuwen, J. Groeneveld, and J. D. Boer, *Physica* **25**, 792 (1959).
- [13] E. Krotscheck and M. L. Ristig, *Phys. Lett. A* **48**, 17 (1974).
- [14] S. Fantoni and S. Rosati, *Nuovo Cimento* **25A**, 593 (1975).
- [15] A. D. Jackson, A. Lande, and R. A. Smith, *Physics Reports* **86**, 55 (1982).
- [16] A. D. Jackson, A. Lande, and R. A. Smith, *Phys. Rev. Lett.* **54**, 1469 (1985).
- [17] E. Krotscheck, R. A. Smith, and A. D. Jackson, *Phys. Rev. A* **33**, 3535 (1986).
- [18] S. Fantoni and S. Rosati, *Nuovo Cimento* **43A**, 413 (1977).
- [19] V. R. Pandharipande and R. B. Wiringa, *Rev. Mod. Phys.* **51**, 821 (1979).
- [20] R. B. Wiringa and V. R. Pandharipande, *Nucl. Phys. A* **299**, 1 (1978).
- [21] E. Krotscheck, *Nucl. Phys. A* **482**, 617 (1988).
- [22] B. L. Scott and S. A. Moszkowski, *Nucl. Phys.* **29**, 665 (1962).
- [23] V. R. Pandharipande and H. A. Bethe, *Phys. Rev. C* **7**, 1312 (1973).
- [24] V. R. Pandharipande and R. B. Wiringa, *Rev. Mod. Phys.* **51**, 821 (1979).
- [25] R. A. Smith and A. D. Jackson, *Nucl. Phys. A* **476**, 448 (1988).
- [26] M. Baldo, A. Polls, A. Rios, H.-J. Schulze, and I. Vidaña, *Phys. Rev. C* **86**, 064001 (2012).
- [27] R. F. Bishop, in *Condensed Matter Theories*, Vol. 10, edited by M. Casas, J. Navarro, and A. Polls (Nova Science Publishers, Commack, New York, 1995) pp. 483–508.

- [28] E. Krotscheck, Phys. Lett. A **190**, 201 (1994).
- [29] H.-H. Fan and E. Krotscheck, Physics Reports **823**, 1 (2019).
- [30] E. Krotscheck, Phys. Rev. B **33**, 3158 (1986).
- [31] A. D. Jackson, A. Lande, R. W. Guitink, and R. A. Smith, Phys. Rev. B **31**, 403 (1985).
- [32] L. J. Lantto and P. J. Siemens, Phys. Lett. B **68**, 308 (1977).
- [33] H. K. Sim, C.-W. Woo, and J. R. Buchler, Phys. Rev. A **2**, 2024 (1970).
- [34] J. W. Clark, in *Progress in Particle and Nuclear Physics*, Vol. 2, edited by D. H. Wilkinson (Pergamon Press Ltd., Oxford, 1979) pp. 89–199.
- [35] E. Krotscheck, J. Low Temp. Phys. **119**, 103 (2000).
- [36] E. Krotscheck and M. Saarela, Physics Reports **232**, 1 (1993).
- [37] J. C. Owen, Phys. Rev. B **23**, 2169 (1981).
- [38] A. L. Fetter and J. D. Walecka, *Quantum Theory of Many-Particle Systems* (McGraw-Hill, New York, 1971).
- [39] H. A. Bethe and J. Goldstone, Proc. R. Soc. London, Ser. A **238**, 551 (1957).
- [40] G. Ripka, Nucl. Phys. A **314**, 115 (1979).
- [41] B. L. Friman, J. Niskanen, and E. M. Nyman, Nucl. Phys. A **383**, 285 (1982).
- [42] D. J. Thouless, *The quantum mechanics of many-body systems*, 2nd ed. (Academic Press, New York, 1972).
- [43] A. Gezerlis, C. J. Pethick, and A. Schwenk, in *Novel Superfluids*, Vol. 2, edited by K. H. Bennemann and J. B. Ketterson (Oxford University Press, 2014) Chap. 22, pp. 580–615.
- [44] A. Gezerlis and J. Carlson, Phys. Rev. C **77**, 032801 (2008).
- [45] H.-H. Fan, E. Krotscheck, and J. W. Clark, J. Low Temp. Phys. **189**, 470 (2017).
- [46] S. Gandolfi, A. Y. Illarionov, K. E. Schmidt, F. Pederiva, and S. Fantoni, Phys. Rev. C **79**, 054005 (2009).
- [47] D. E. González Trotter, F. Salinas, Q. Chen, A. S. Crowell, W. Glöckle, C. R. Howell, C. D. Roper, D. Schmidt, I. Šlaus, H. Tang, W. Tornow, R. L. Walter, H. Witała, and Z. Zhou, Phys. Rev. Lett. **83**, 3788 (1999).
- [48] H. A. Bethe, B. H. Brandow, and A. G. Petschek, Phys. Rev. **129**, 225 (1963).
- [49] E. Krotscheck, Nucl. Phys. A **293**, 293 (1977).
- [50] J. Wambach, T. Ainsworth, and D. Pines, Nucl. Phys. A **555**, 128 (1993).
- [51] A. Sedrakian and J. W. Clark, “Superfluidity in nuclear systems and neutron stars,” (2018),

arXiv:1802.00017.

- [52] E. Krotscheck, Phys. Rev. A **15**, 397 (1977).
- [53] A. D. Jackson and R. A. Smith, Phys. Rev. A **36**, 2517 (1987).
- [54] C. E. Campbell, R. Folk, and E. Krotscheck, J. Low Temp. Phys. **105**, 13 (1996).
- [55] E. Krotscheck and J. W. Clark, Nucl. Phys. A **333**, 77 (1980).
- [56] J. Bardeen, L. N. Cooper, and J. R. Schrieffer, Phys. Rev. **108**, 1175 (1957).
- [57] E. Krotscheck, J. Paaso, M. Saarela, K. Schörkhuber, and R. Zillich, Phys. Rev. B **58**, 12282 (1998).
- [58] E. Krotscheck, Phys. Rev. A **26**, 3536 (1982).